The Micrometeoroid Complex and Evolution of the Lunar Regolith

F. Horz, D. A. Morrison
NASA/Johnson Space Center
Houston, Texas

D. E. Gault, V. R. Oberbeck, W. L. Quaide, J. F. Vedder
NASA/Ames Research Center
Moffett Field, California

D. E. Brownlee
University of Washington
Seattle, Washington

J. B. Hartung
Max Planck Institut fur Kernphysik
Heidelberg, Germany

Mirometeoroid Complex: The interaction of the micrometeoroid complex with the lunar surface is evidenced by numerous glass-lined microcraters on virtually every lunar surface exposed to space. Such craters range in size from $< .1\mu$m to approximately 2 cm in diameter. With the use of small-scale laboratory cratering experiments for "calibration," the observed crater-sized frequency distributions may be converted into micrometeoroid mass distributions. These "lunar" mass distributions are in essential agreement with satellite data for masses $> 10^{-12}$g. However, for masses $< 10^{-12}$ g there is considerable discrepancy. A radiation pressure cutoff does not exist because masses as small as 10^{-15} g can be observed. The absolute flux of micrometeoroids based on lunar rock analyses averaged over the past few 10^6 years is approximately an order of magnitude lower than presentday satellite fluxes; however, there is indication that the flux increased in the past 10^4 years to become compatible with the satellite data. Furthermore, there is detailed evidence that the micrometeoroid complex existed throughout geologic time.

Some physical properties of micrometeoroids may be deduced by comparing lunar crater geometries with those obtained in laboratory experiments. The preponderance of circular outlines of lunar microcraters necessitates equidimensional, if not spherical, micrometeoroids. Irregular shapes such as whiskers, needles, platelets, rods, etc.—postulated in the past—do not contribute substantially to the micrometeoroid population and are rare, if not absent. The depth/diameter ratios of lunar microcraters are compatible with micrometeoroid densities of 2 to 4 g/cm^3; densities < 1 g/cm^3 can be excluded. These findings have astronomical significance with respect to comets, i.e., the source area for micrometeoroids.

Regolith-Dynamics: Monte Carlo-based computer calculations, as well as analytical approaches utilizing probabilistic arguments, were applied to gain insight into the principal regolith impact processes and their resulting kinetics. Craters 10 to 1500 m in diameter are largely responsible for the overall gowth of the regolith. As a consequence the regolith has to be envisioned as a complex sequence of discrete ejecta blankets. Such blankets constitute first-order discontinuities in the evolving debris layer. The micrometeoroid complex then operates intensely on these fresh ejecta blankets and accomplishes some degree of mixing and homogenization. True mixing, however, can be accomplished only in an uppermost layer of approximately 1-mm thickness, before a new ejecta event covers this

layer and effectively removes it from the zone of active reworking. While, e.g., a layer 1 cm in depth is turned over only one time in approximately 10^7 years, the uppermost 1 mm of that surface has been turned over already 250 times and the uppermost .1 mm more than 2000 times during the same period. Therefore the lunar regolith becomes rapidly quiescent with depth. Though the micrometeoroid bombardment is extensive, a startigraphic sequence may readily be preserved, as evidenced in returned core tube materials. The erosion of lunar rocks caused by micrometeoroids is calculated at .3 to .6 mm per 10^6 years. The mean surface residence time of a rock of 1 kg in mass is in the order of 3×10^6 years, before it will be catastrophically destroyed by rupturing due to the impact of large micrometeoroids. This catastrophic destruction is far more effective than single particle abrasion in obliterating a lunar rock specimen. Due to the vagarities of the random impact process, caution is necessary to delineate regolith dynamics from lunar sample analyses that are not based on a statistically significant number of observations.

With increasing resolution of lunar surface photographs prior to actual sample return, it became more and more obvious that meteoroid impact had played a substantial role in the evolution of the lunar surface. It was discovered that meteoroid impact had operated on scales from hundreds of km down to a few cm (ref. 1). However, immediately upon cursory inspection of returned rocks it was learned that impact processes also occurred on still smaller scales: the ubiquitous presence of glass-lined lunar microcraters was ample evidence that virtually every lunar surface exposed to space was also subjected to the bombardment of micrometeoroids. In the meantime numerous laboratory investigations revealed that many properties of the lunar regolith are either directly or indirectly dominated by impact processes far beyond the original expectations. A proper understanding of many regolith processes therefore depends critically upon an understanding of the regolith impact history.

A thorough understanding of this history is possible only by combining lunar observational data, laboratory impact experiments, and theoretical calculations. This report attempts to summarize such analyses. We will first discuss observational evidence of lunar microcraters and its implications to the micrometoroid complex, including some astronomical consequences. We then will present some analytical and computer-based calculations that will aid in the understanding of some principal regolith processes as well as their kinetics. Due to limited space some detailed argumentation cannot be presented, and the reader must be referred to the original reports. In addition, a multitude of other interesting observations and interpretations had to be deleted. We attempted, however, to present the most important aspects of the impact process as we understand them today.

Lunar Data of the Micrometeoroid Complex

MICROCRATER-MORPHOLOGY

Glass surfaces are by far the most suitable materials to study micrometeoroid impacts, because in comparison with crystalline rocks and breccias, they are usually smooth and observational conditions are optimized (fig. 1). Furthermore, glasses are also the best investigated materials in small-scale laboratory cratering simulations. Thus—unless specified—the detailed morphology data, crater-size frequency distributions, and associated flux considerations are derived from lunar glass surfaces only.

Microcraters on lunar glass surfaces may range in diameter from less than .1μm up to approximately 2 mm; on crystalline rocks craters as large as 20 mm in pit diameter were observed. Crater morphology differs characteristically as a function of absolute crater diameter (refs. 2–5). Craters smaller than 1μm are cup-shaped, glass-lined depressions—termed "pit"—with a pronounced rim of molten target material (fig. 2(a)). Craters between 1μm and 10μm in pit diameter (figs. 2(b) and 2(c)) are transitional between the above morphology and that typical for craters

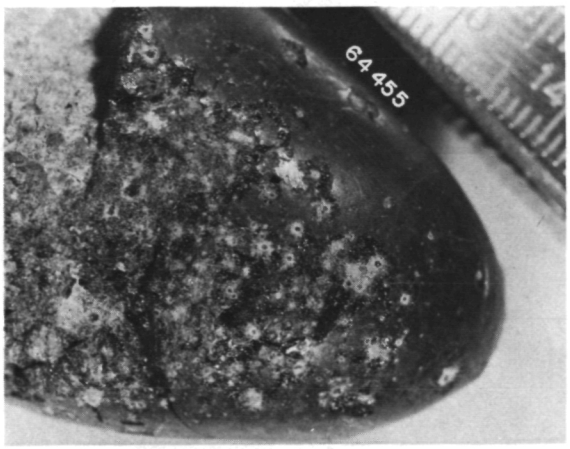

Figure 1.—*Large glass-coating on lunar rock 64455 with abundant microcraters. All structures are above 5 μm in diameter and therefore display characteristic spall zones. Close to the fracture zone exposing the underlying anorthositic substrate, the crater densities are very high and in approximate equilibrium. (Sidelength of picture: 3.2 cm.)*

larger than 10μm. When above 10μm in diameter, they not only possess a central glass-lined pit but also a concentric spall zone (fig. 2(d)). The spall zone may or may not be totally spalled off for craters between 10μm and 50μm, but all craters above 50μm in diameter have a completely developed spall zone. Morrison et al. (ref. 5) delineated the following relationship: $D_S = 2.37 \times D_P^{1.07}$, where D_S is the spall zone and D_P the pit diameter.

For comparison, identical structures produced in the laboratory are illustrated in figures 2(e) and 2(f). Laboratory crater studies performed by electrostatic particle accelerators (refs. 6–13) indicate that a glass-lined pit is produced only at projectile velocities exceeding 3 km/s. The development and extent of a spall zone characteristic for the larger lunar craters requires velocities in excess of 5 km/s.

PHYSICAL PROPERTIES OF MICROMETEOROIDS

Laboratory simulations by Mandeville and Vedder (ref. 9); Kerridge and Vedder (ref. 14); Vedder and Mandeville (ref. 12); and Mandeville (ref. 13) have demonstrated that the outline of the central pit crater is controlled by projectile shape and angle of incidence and that the crater depth is dependent on projectile density and impact velocity.

Brownlee et al. (ref. 15) measured crater-circularities from Scanning Electro-Microscope (SEM) photographs that were taken with the electron-optical axis normal to the cratered surface. A "circularity index" was defined as the ratio A_m/A_c, where A_m is the area measured along the inferred intersection of the surrounding target surface with the inside of the pit rim, while A_c is the area of the smallest circle which just encloses A_m. Circularity indices measured for 131 micron-sized craters demonstrate the rarity of highly noncircular pits (fig. 3). Many of the noncircular craters in figure 3 are elongated and shallow, indicating that they were produced by oblique impact rather than highly irregular projectiles (refs. 15 and 16). By comparison with laboratory simulations using irregular projectiles (ref. 14), it is concluded that highly nonspherical shapes such as rods or platelets are rare or nonexistent in the micrometeoroid complex. If dust grains were modeled as prolate ellipsoids, then the observed crater circularities suggest an average length to width ration of < 2.

Depth/diameter ratios were determined for 70 craters (ref. 15) by use of the contamination line profiling technique of Vedder and Lem (ref. 17) and parallax measurements from SEM stereo photos. The crater depth/diameter ratios refer to the maximum pit depth below the original uncratered surface divided by the mean diameter of the inside of the pit rim. Figure 4 illustrates the results of 70 lunar craters in histogram form together with laboratory cratering data of Vedder and Mandeville (ref. 12). Because the laboratory data do not extend beyond 13 km/s impact velocity and because the velocity distribution of small meteoroids is not well known, it is not possible to determine exact particle densities. It is obvious, however, that the data are entirely inconsistent

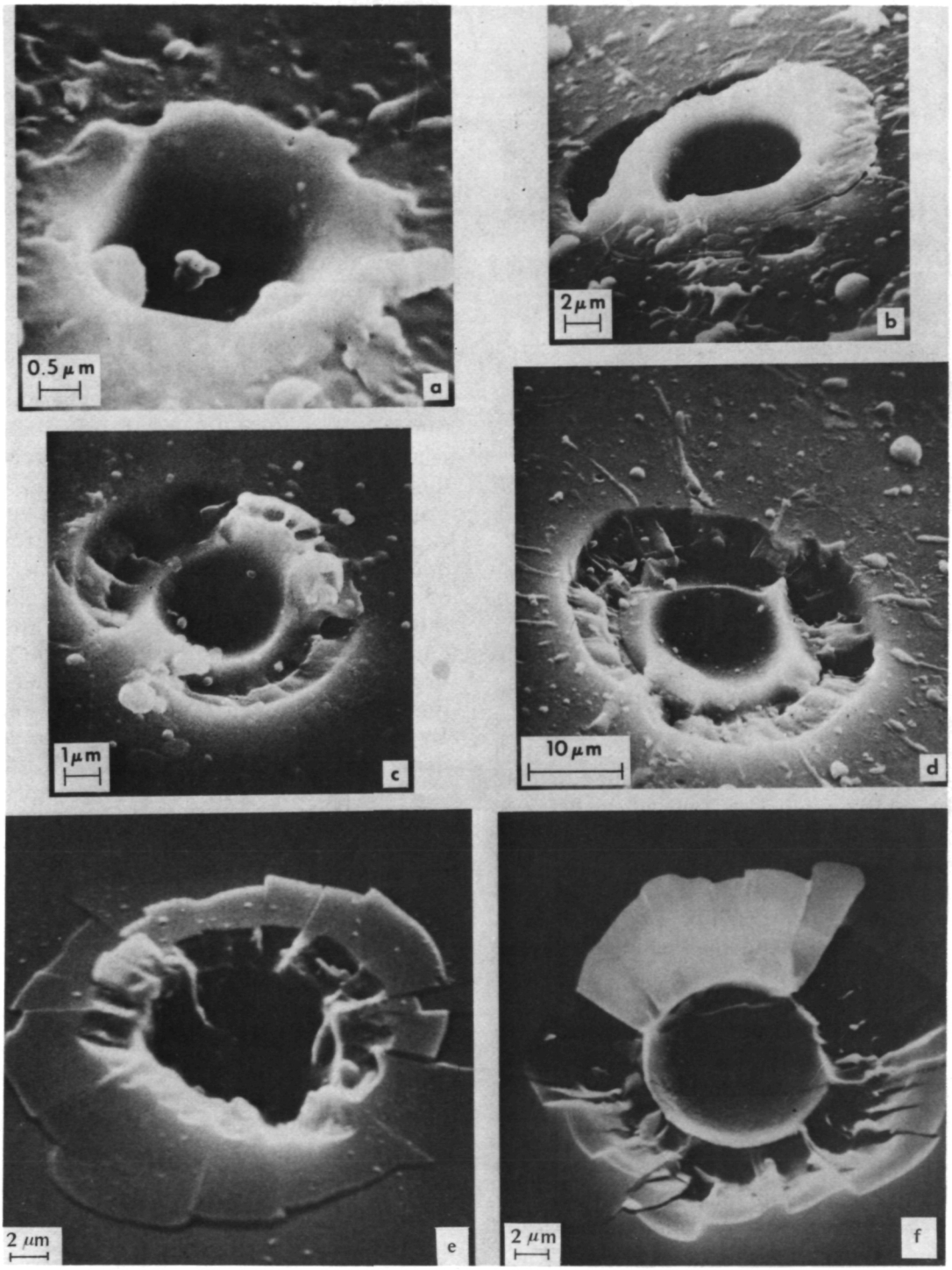

Figure 2.—*Typical lunar experimental microcraters on glass surfaces. Note the change of crater morphology with size: (a) very small lunar microcrater that displays neither concentric fractures nor a spall zone (note the raised, glassy rim); (b) lunar crater that displays concentric fracture zone indicative of incipient spallation; (c) lunar crater with partially developed spall zone; (d) lunar crater with completely developed spall zone; (e) experimental crater (Al-projectile into soda lime glass; impact velocity: 9.9 km/s); and (f) experimental crater (polystyrene projectile into soda lime glass; impact velocity: 5.7 km/s. Note shallow crater depth and compare with 2(a)–(e)).*

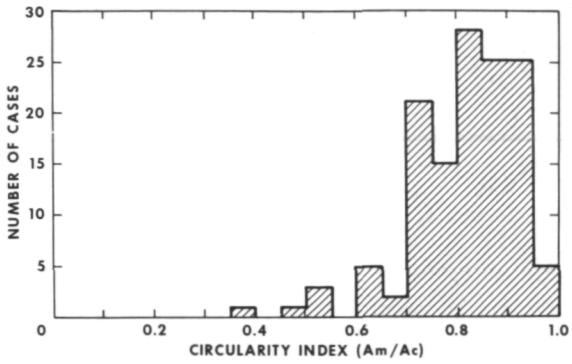

Figure 3.—*Histogram of the circularity index of 131 microcraters ranging in size from .2 to 80 μm in diameter (rock 15286). Though not illustrated, the circularity index is independent of pit crater diameter.*

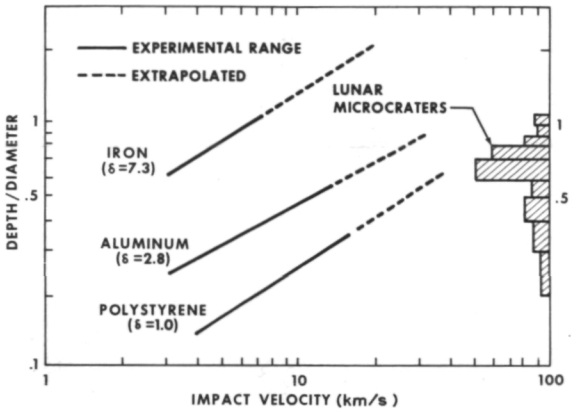

Figure 4.—*Experimentally determined depth/diameter ratios using projectiles with densities from 1 to 7 g/cm³ and impact velocities from 3 to 13 km/s. The inserted histogram on lunar depth/diameters is based on 70 craters.*

with micrometeoroid densities less than unity. The rarity of deep craters also appears to exclude the possibility that a significant fraction of particles could have densities as high as iron. Figure 4 apparently implies that most micrometeoroids ($< 50\mu$m in diameter) have densities in the 2 to 4 g/cm³ range, if one assumes an average impact velocity of 20 km/s. Even for velocities between 10 and 30 km/s, the above densities are approximately valid.

Only $\approx$ 10 percent of the total crater population may offer different interpretations. Of those exceptions, the so-called "pitless" craters are by far the most abundant ($\approx$ 80 percent). They do not possess a glass-lined pit (fig. 5(a)) and could be interpreted as low-velocity, "secondary" craters. However, as illustrated in figure 5(b) and as observed numerous times, there is strong evidence that many "pitless" craters did indeed have a glass-lined pit, which was spalled off either during crater formation or thereafter (ref. 18). Thus, many of these structures are also potential candidates for a "primary" origin (ref. 19). Another exceptional crater type, termed "multiple pit crater," is illustrated in figure 5(c); figure 5(d) documents a laboratory equivalent produced by an agglutinate of minute glass spheres (ref. 12). Consequently it is conceivable that "multiple pit craters" are indeed caused by projectiles of low density and nonhomogeneous mass-distribution, i.e., "aggregate" structure; however, they are rare exceptions and far less frequent than suggested by Verniani (ref. 20), Hughes (ref. 21), and many others.

CRATER POPULATIONS ON LUNAR ROCKS

In analogy to large-scale lunar surfaces (Gault (ref. 22); Shoemaker et al. (ref. 1), and others), two basic types of crater populations need to be distinguished: (a) "production" and (b) "equilibrium" populations. By definition, "production populations" are limited to rock surfaces of low, absolute crater densities, i.e., of short exposure periods. With time, more and more impacts will occur in already cratered areas until finally the surface becomes so densely cratered that each new event will destroy an already existing one. Such a surface has reached "equilibrium." "Transition populations" are intermediate between "production" and "equilibrium" conditions. Most lunar rocks are either in "transition" or "equilibrium" condition; genuine "production populations" are rare.

Because production surfaces exclusively

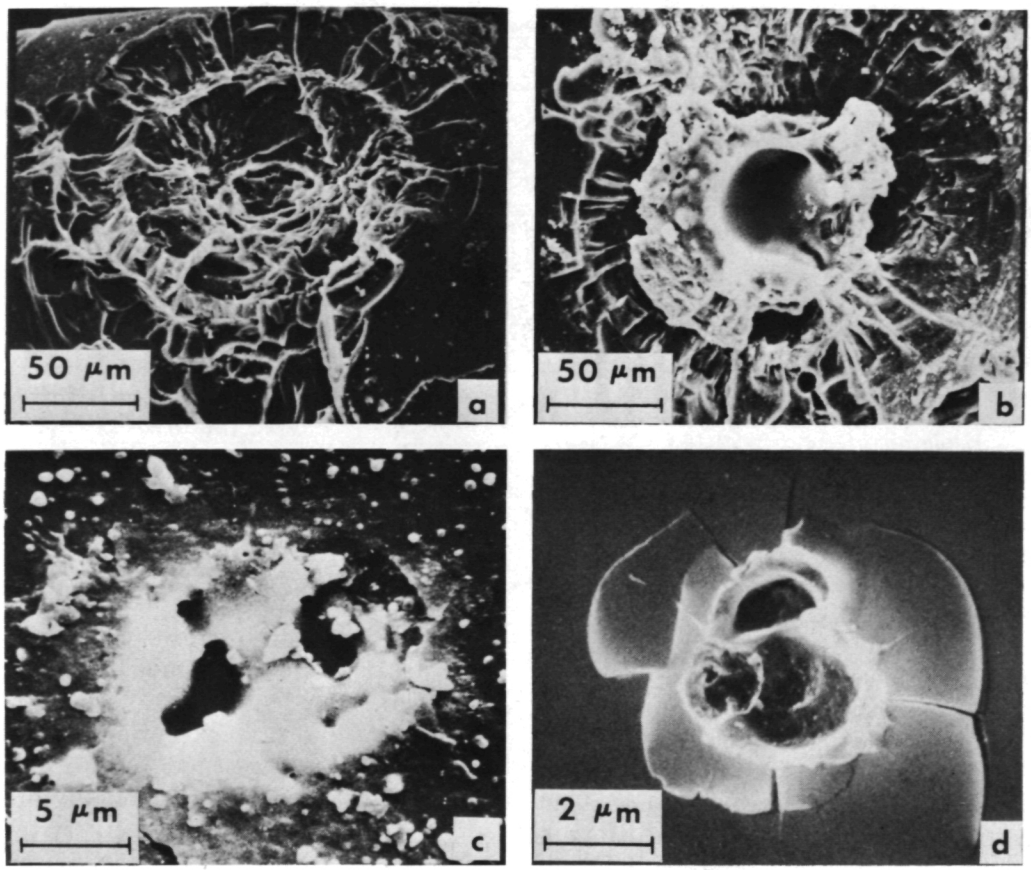

Figure 5.—*Unusual craters: (a) "pitless" lunar crater (note the similarities and possible transition to crater 5(b)); (b) similar sized lunar crater* with *pit (note that spallation action was severe enough to undercut the glass-lined pit, leaving it barely attached to the crater bottom); (c) "multiple pit" crater on lunar glass surface 15286); and (d) "multiple pit" crater produced in the laboratory.*

display a complete record of all craters produced, *only they are suitable* to deduce mass-frequencies and the flux of micrometeoroids.

Cumulative crater size distributions for "production populations" on samples 12054 (ref. 4) and 60015 (ref. 23) are shown in figure 6; though other genuine "production populations" were investigated, the two curves illustrated are considered the best available over the size range indicated. The absolute crater densities for the two samples differ by almost a factor of 2, reflecting different times and/or geometry of exposure. The relative crater size frequency, however, is nearly identical.

Figure 7 illustrates "production" data resulting from SEM studies. The relative frequencies were normalized to surface 15205 at a pit diameter of 1μm. The illustrated data are considered the best available. The differences in the distributions and the presence of an inflection at pit diameters between 1μm and 10μm are subject to a variety of interpretations. They will be discussed later.

Because the rock surfaces that have reached "transition" and/or "equilibrium" conditions are less suitable for study of the micrometeoroid complex, they will not be treated extensively here (refs. 5, 23, 25, 26, and 27). However—if coupled with solar flare track exposure ages—they may still contribute to the flux determination of micrometeoroids; *minimum* fluxes may be obtained, because a number of the craters produced are destroyed and not observable anymore.

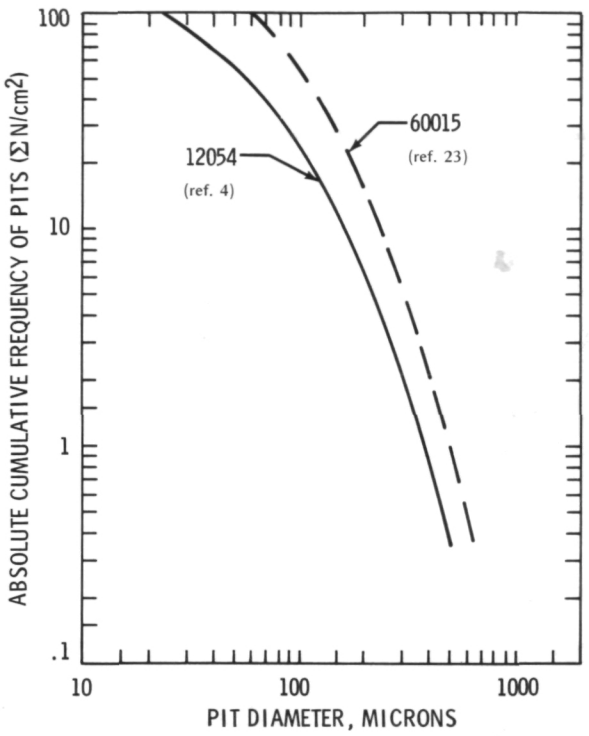

Figure 6.—*Typical binocular crater-size frequency distributions for lunar glass surfaces in production state (12054 is based on 960 craters; 60015 is based on 665 craters).*

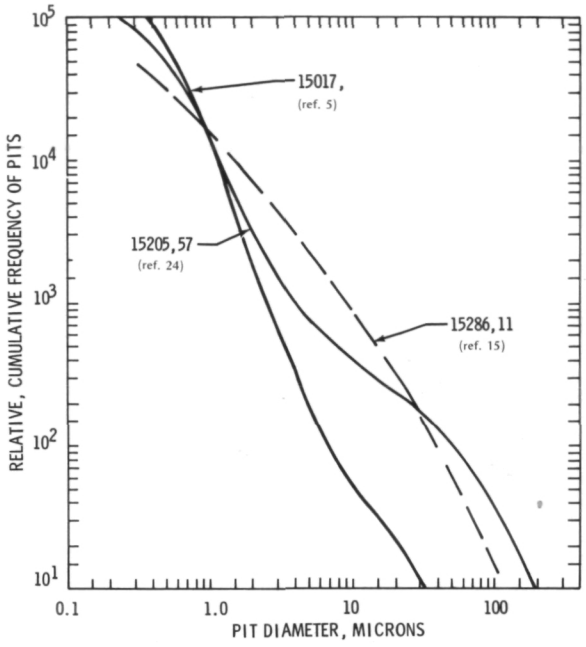

Figure. 7.—*Typical scanning electron microprobe crater-size frequency distributions for small microcraters on lunar glass surfaces in production state (15205 is based on ≈ 1100 craters, 15286 on ≈ 500, and 15017 on ≈ 300).*

MASS-FREQUENCY OF MICROMETEOROIDS

Crater simulation experiments provide the only basis to obtain information concerning the mass distribution of micrometeoroids by converting crater dimensions into projectile parameters. The physical processes governing impact cratering are complex and presently not understood in great detail, despite considerable laboratory work. Especially, the energy partitioning for small- and large-scale cratering and the effects of target strength, gravitational forces, and varying impact velocities, i.e., appropriate "scaling laws," are still subject to experimental work that ultimately will result in a theoretical understanding. Therefore, extrapolations from laboratory data may allow the use of a *variety* of empirical calibration approaches.

Four basic calibration techniques for microcraters are currently in use (fig. 8). Two are based on electrostatic dust accelerator experiments (refs. 6, 9, 24, and 30), and two calibration techniques utilize results from ballistic ranges (refs. 28 and 31), while Nagel (ref. 29) employed a lithium plasma gun (for more detail, see ref. 16).

Relative crater-size frequency distributions ranging from .1 to almost 1000 microns in pit diameter may be constructed from the data presented in figures 6 and 7 by normalizing the absolute crater densities with respect to exposure time, exposure geometry, and surface area. An important assumption underlying such a normalization is that these relative frequencies remained constant with time, because surfaces of different crater

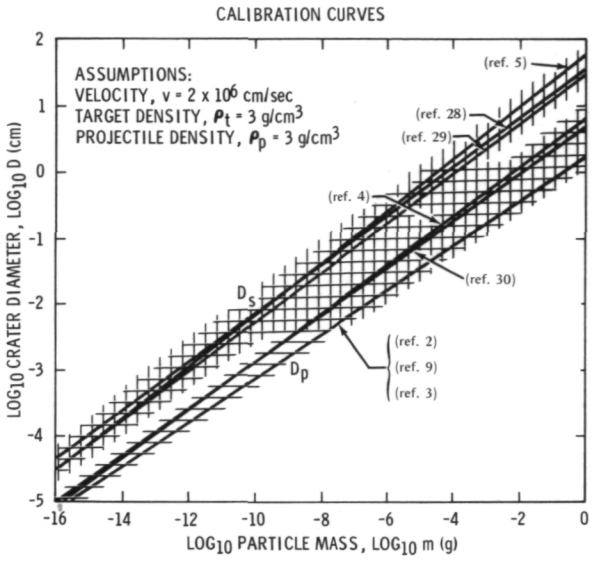

Figure 8.—*Various calibration methods presently in use to derive micrometeoroid masses from measured pit diameters* (D_p) *or spall diameters* (D_s). *The ratio* D_s/D_p *is variable from rock to rock with values between 3.8 and 4.5 on lunar glasses. Note that agreement between various techniques is close, if a* D_s/D_p *of 4.5 is applied.*

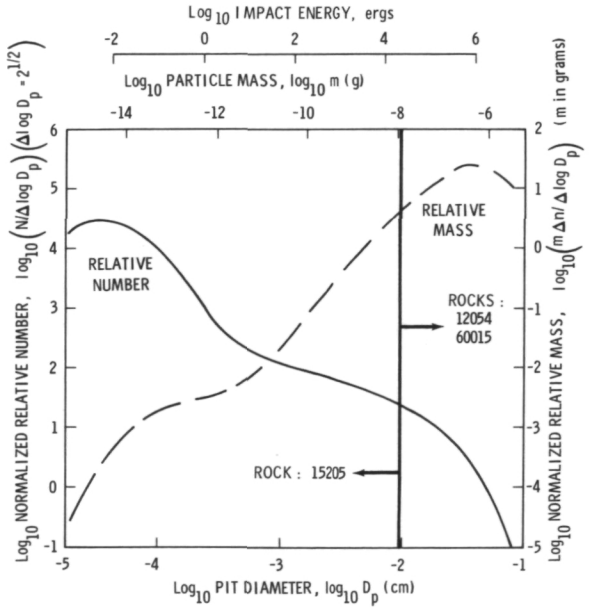

Figure 9.—*Differential frequency of pit diameters and their corresponding particle mass and energy distributions. The binocular data (12054, 60015) and SEM data (15205) are joined at a pit diameter of 100 μm as indicated.*

densities, i.e., different absolute exposure times, need to be normalized. Figure 9 shows such a normalized, differential crater frequency distribution based on glass-surfaces 12054, 60015, and 15205. The corresponding mass- and energy-scales are based on the calibration by Gault (ref. 28) as shown in figure 8. For masses $> 10^{-10}$g (= impact energies above 200 ergs) this distribution is in basic agreement with that obtained by satellite- and ground-based measurements (refs. 32 and 33). Though the irregularity of the distribution at lower masses will be more thoroughly discussed later, it can already be seen that

1. Particles in the 10^{-15} to 10^{-13} g range are most numerous.
2. The bulk of the meteoroid mass or energy impacting the Moon is confined to particles 10^{-8} to 10^{-3} g in mass (see also refs. 4 and 34).

FLUX OF MICROMETEOROIDS

Micrometeoroid fluxes are obtained by correlating absolute crater densities with the

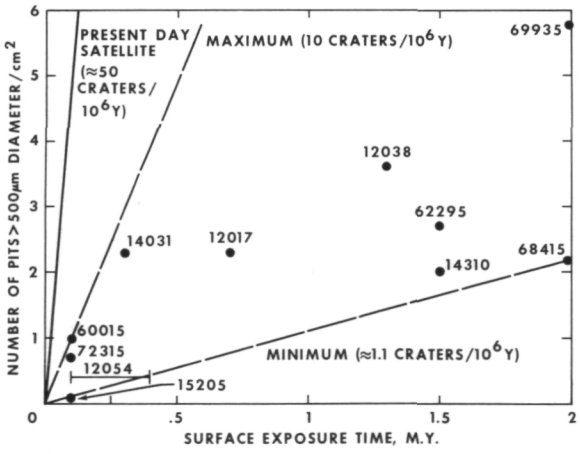

Figure 10.—*Correlation of surface residence times of specific rocks mostly determined with solar flare tracks (see table 1) and absolute frequency of pit craters > 500 μm in diameter/cm². A straight line going through the origin establishes the crater production rate, i.e., the flux of micrometeoroids* $> 2 \times 10^{-7}$ *g. A best estimate for the average flux over the past* 10^6 *years is* $\approx$ *5 pits/cm².*

absolute exposure age. A summary of such correlations for binocular crater counts on selected rocks is illustrated in figure 10, with the cumulative crater frequency for pits above 500μm in diameter. Most data points shown lie below possible correlation lines and therefore are in or approaching equilibrium with respect to cratering. A correlation line corresponding to a crater production rate of five pits with diameters equal to or greater than 500 microns per cm^2 per million years lies within a factor of 2 of data for 12054, 12017, 12038, and 14301. Upon visual inspection of these samples, only rock 12038 was not clearly in production with respect to cratering. A factor of 2 is the estimated uncertainity in the solar flare track method used for the exposure time measurements.

Another approach to measure the meteoroid flux and possible changes with time has been pursued by Hartung et al. (ref. 35). Separate solar flare track exposure ages were determined for 56 individual pit craters larger than 20μm on rock 15205. The results illustrated in figure 11 indicate that the formation ages of these craters are not uniformly distributed; significantly more craters are produced during the last 10 000 years. Thus it appears that the present-day micrometeoroid flux is enhanced over that of the past 10^4 to 10^5 years by slightly more than an order of magnitude. The values obtained for the past 3000 years are in good agreement with present-day satellite measurements (refs. 33 and 34).

Discussion of the Micrometeoroid Complex

IMPLICATIONS OF PHYSICAL PROPERTIES

On the basis of laboratory cratering experiments, the morphologies of microcraters are interpreted to indicate that they were formed by equidimensional, nonporous projectiles of densities between 2 and 4 g/cm^3, which impacted with velocities in excess of 5 km/s. These results are in part contrary to popular hypotheses and they may have

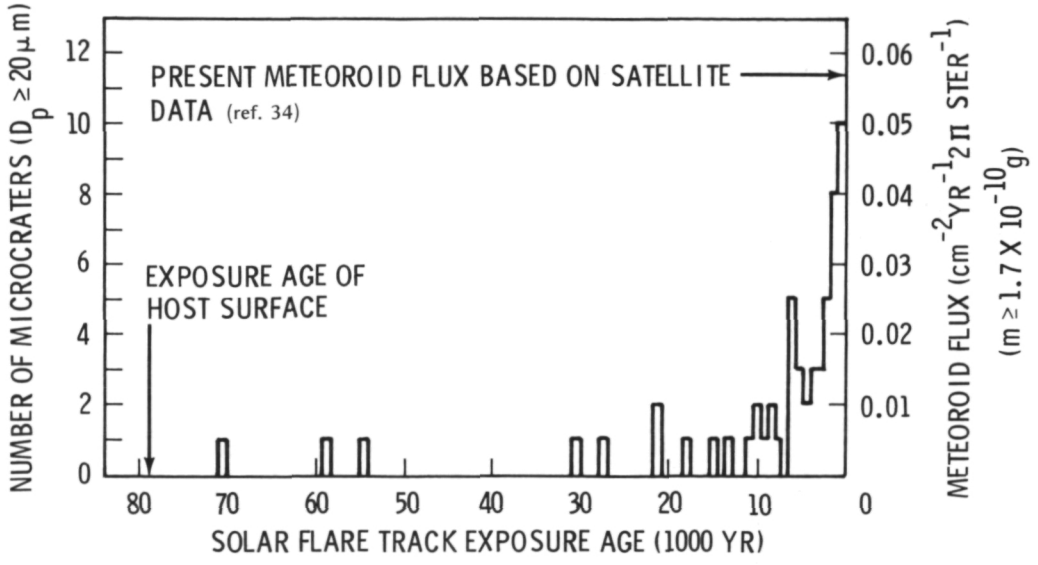

Figure 11.—*Preliminary formation ages of 56 individual microcraters ranging in size from 20 to 300 microns in pit diameter on glass surface 15205,51. Note the steep increase in crater production rate between 0 and 10^4 years, corresponding to a twofold increase every 3000 years.*

some significant astronomical consequences.

A cometary origin for micrometeoroids is strongly suggested by a variety of independent analyses (e.g., refs. 33 and 36). The particulate matter within comets is believed to represent unfractionated, solar abundances similar to Type 1 carbonaceous (CI) chondrites. Our mass densities are entirely consistent with CI chondrites, the constituents of which range in density from approximately 1.5 g/cm^3 for aggregates of phyllo-silicates to magnetite grains of 5g/cm^3 in density (ref. 37).

Much lower densities with an average of .5 to .8 g/cm^3 have been suggested for the somewhat larger meteors, i.e., particles $> 10^{-6}$ g (refs. 20 and 21). Though our detailed analysis of crater morphologies is confined to craters below 100μm in diameter, i.e., particles $< 10^{-8}$ g, even pit craters larger than 1 cm, caused by particles of approximately 10^{-3} g, display qualitatively the same morphologies. Though precise laboratory calibrations are not available for such large structures, we suggest that most particles of 10^{-6} to 10^{-3} g may also have a density of more than unity.

The equidimensional character of micrometeoroids may also have significant astronomical implications, if we accept a cometary source. Traditionally it is suggested that such materials are similar if not identical in chemistry and shape to grains found in carbonaceous chondrites, because they are believed to represent primordial condensates from similar environments in the solar nebula. These grains are thought to be vapor growth products of highly nonspherical shape like platelets, rods, and whiskers (refs. 14, 38, 39, and 40). Such grains were observed in a variety of carbonaceous meteorites, e.g., Allende, which is thought to be a fine example of "early condensates" (ref. 41). Clearly the microcrater circularities are incompatible with such elongated grains. These findings either imply that the postulated grain shapes are incorrect and virtually nonexisting in the environment of comet formation or that the micrometeoroid complex is also the result of multiple collisional events prior (!) to incorporation into cometary matrices. Recent developments in meteorite research provided strong evidence that collisional processes in the early history of the solar system may have played a dominant role.

Regardless of what caused the micrometeoroids' equidimensional if not spherical shape, needles, platelets, rods, whiskers, and other elongated or irregular particles seem not to make up a significant part of cometary silicates, if one accepts at all a cometary source area. The possibility that most of these particles constitute debris of collisional processes during accretion, rather than primary condensates, cannot be excluded.

MASS-FREQUENCY

The frequencies of micrometeoroid masses ranging from 10^{-15} to 10^{-3} g are summarized in figure 12, together with a variety of satellite- and earth-based measurements. Two types of microcrater frequencies are observed: that displayed by samples 15205, 15076, and 15017; and that of sample 15286. Though experimental conditions (most dominantly target-smoothness and total number of craters counted) may be responsible for subtle differences of the first type, the different behavior of 15286 seems beyond statistical error. Rock 15205 is based on 950 craters and sample 15286 on 500 craters. Thus, two questions remain: (1) Why are there two different frequency types? and (2) What causes an apparent bimodal mass distribution?

Sample 15286 is unique, though there are other samples (e.g., 12024,81 and 14257,F (ref. 30)) that may be similar. Their different mass-frequencies may be caused by extreme solid angles of exposure (ref. 23) that effectively influence the energy distribution, because of the increased effects of oblique impact (ref. 28). It is also conceivable that such surfaces were essentially pointing toward lunar North, i.e., out of the ecliptic plane, where they potentially could intercept a different population of cosmic dust than within the ecliptic plane.

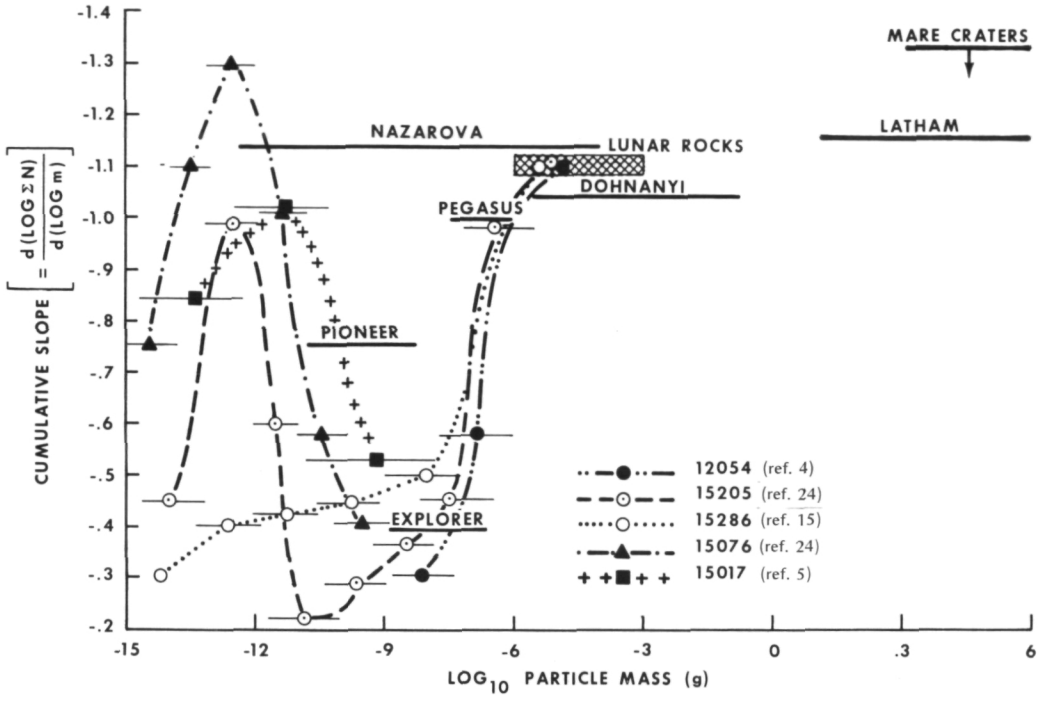

Figure 12.—*Comparison of the cumulative mass-frequency* slopes *of a variety of observational techniques, but, in particular, of five well-documented lunar glass surfaces. Most individual satellite data do not give a differential flux; the position of the satellite data was constructed by extrapolating the slope from the cummulative mass-frequency curve of Dohnanyi (ref. 33, fig. 1). The length of the bars indicates the mass-range over which the corresponding slope is valid.*

Curves 15205, 15076, and 15017 are believed to be typical for micrometeoroids impacting the Moon, simply because such distributions are the most frequent ones. Samples 60502,17; 15927,3; 15301,79 (ref. 24); and 15015 (ref. 5) yield similar results. The cause of this apparent bimodal mass distribution is presently unknown. However, it is conceivable that the larger masses represent the cometary particle population that is spiraling *toward the Sun*. During and upon solar approach, individual particles may suffer fragmentation as well as melting and/or vaporization; both processes would result in numerous particles of very small sizes. Upon close solar approach they may be propelled *away from the Sun* again by solar radiation and have a second opportunity to encounter the lunar surface (refs. 36 and 42).

Subtle differences in crater populations may yet be caused by a completely different mechanism. Morrison et al. (ref. 5) and Blanford et al. (ref. 43) report that lunar rock surfaces are significantly modified on the micron scale by the accretion of regolith particles; most dominantly, disk-shaped, glassy splashes and droplets. These accretionary objects are so numerous that they accumulate obviously at a faster rate than the surface is destroyed by microcraters. Given sufficient time they may even build up layers of a few microns in thickness, giving some of the hand specimens a typical, patinated appearance. Thus a "constructive" accretion process is competing with the "destructive" cratering process and the micron-size crater population may be somewhat modified. The unambiguous presence of particles below 10^{-15} g in mass, however, negates the existence of a radiation pressure cutoff. According to Gindilis et al. (ref. 44), the lack of such a cutoff is highly compatible

with particle densities of 2 to 4 g/cm^3, i.e., with silicates, for which gravitational forces appear to dominate radiation pressure. This result corroborates our conclusions about particle densities.

Figure 12 also illustrates one fundamental advantage of lunar glass-surfaces as micrometeoroid detectors: at present, the lunar rock detector spans 12 orders of magnitude in mass and thus possesses a "dynamic range" duplicated nowhere. The potential identification of a bimodal size distribution is only due to such a large dynamic range.

Additional work with carefully selected samples is required to clarify what causes the two basic frequency types and the apparent bimodal distributions. The above explanations have to remain tentative until carefully selected and precisely oriented surfaces are investigated in detail.

MICROMETEOROID FLUX

A detailed comparison of micrometeoroid fluxes derived from lunar sample analyses and satellite measurements is presented in figure 13. It is impossible to discuss each detail and thus we offer a few general comments only, quoting Hörz et al. (ref. 16):

> The moon is a rotating sampler, and the directional distribution of micrometeoroids is extremely non-uniform as shown by Berg and Grün (1973) (ref. 48) and Hoffmann et al. (1973) (ref. 47). Accordingly, the meteoroid flux differs about 3 orders of magnitude between the direction of the earth's apex and anti-apex. Furthermore, particles $> 10^{-12}$ g are collected almost exclusively during the apex orientation of the Pioneer and HEOS sensors. Hence, in this mass range, also the Moon may collect particles from only the apex direction. As a consequence, a "detector" on the rotating lunar surface can "register" meteoroid impacts effectively only part of the time. Therefore, fluxes derived from lunar crater statistics may have to be increased by as much as a factor of π for comparison with satellite data that were taken in the apex direction. Also, apex-pointing data generally have been corrected upward to a standard 2π-sterad exposure angle, assuming an isotropic flux. Thus, an actual anisotropy (as reported by the HEOS and Pioneer experiments) leads to an overestimation of the flux. Therefore, the satellite results seem to represent an upper limit for the flux.
>
> The "apex" particles show an average impact velocity of only 8 km/sec (Hoffmann et al., 1973) (ref. 47). The fluxes from lunar rocks, however, are calculated with a standard velocity of 20 km/sec. The necessary corrections will increase the projectile masses and thereby effectively enhance the Moon-based flux for masses $> 10^{-10}$ g by a factor of approximately 5.
>
> The situation for masses $< 10^{-12}$ g is highly complex. Berg and Grün (1973) (ref. 48) have reported that most events of these masses occur with particles that have relative velocities of at least 50 km/sec. The lunar flux curves given for these masses in fig. 12 are, however, based on a 20 km/sec impact velocity; if corrected to 50 km/sec, they will shift towards smaller masses, possibly as much as a factor of 10.

As a consequence, the fluxes derived from lunar crater statistics may agree within the order of magnitude with direct satellite results if the above uncertainties in velocity and directional distribution are considered.

Figure 14 presents some basic constraints derived from a variety of independent lunar studies on the flux of micrometeoroids and larger objects. The only direct measurements are the impact events registered by the Passive Seismic Experiment (ref. 62) and the micrometeoroids encountered by the spacecraft windows (ref. 57). Upper limits on the flux can be derived from more cratering rate (refs. 63, 64, and 65). Accordingly, the flux over the past 3.0×10^9 years has remained fairly constant. The "geochemical" evidence is based on the abundance of siderophile trace elements indicative of type and

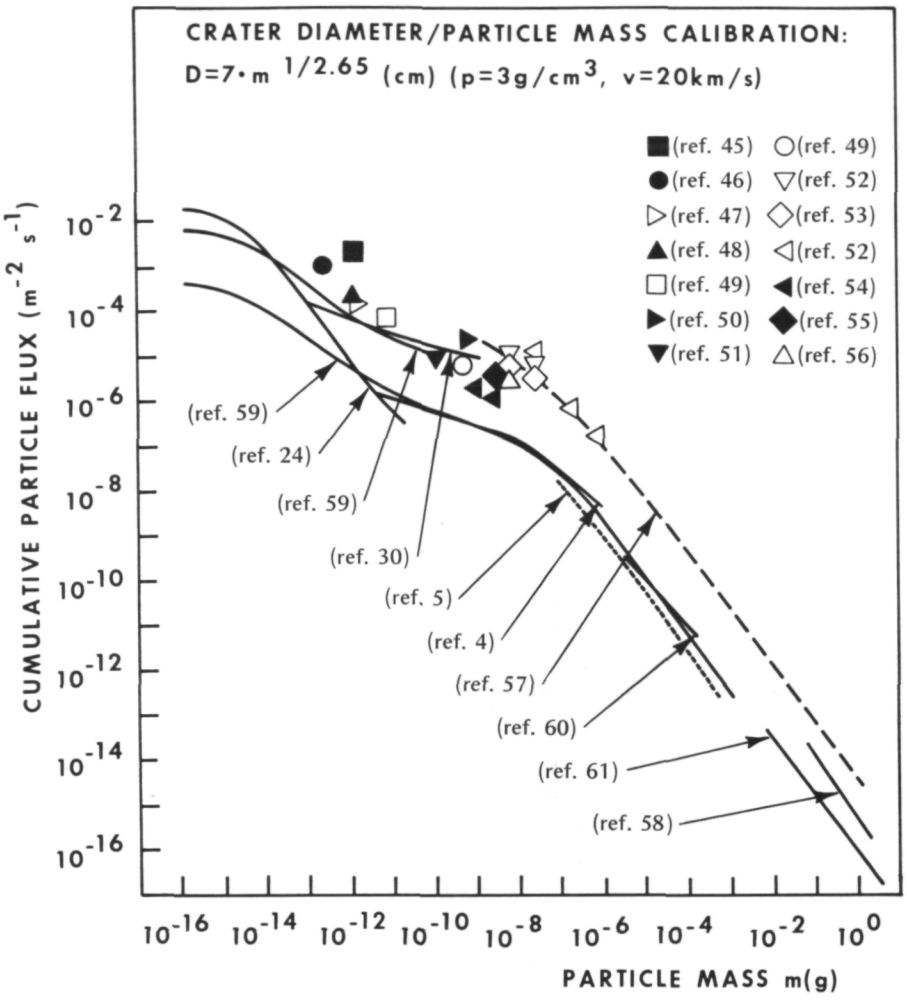

(ref. 4) = Moon (Hartung et al., 1972b)
(ref. 5) = Moon (Morrison et al., 1973)
(ref. 24) = Moon (Schneider et al., 1973)
(ref. 30) = Moon (Neukum et al., 1972)
■ (ref. 45) = OGO II, IV (Nilsson et al., 1969)
● (ref. 46) = OGO III (Alexander et al., 1972)
▷ (ref. 47) = HEOS 2 (Hoffmann et al., 1973, apex)
▲ (ref. 48) = Pioneer 8 (Berg and Grun, 1973)
○ (ref. 49) = Mariner II (Alexander et al., 1965)
□ (ref. 49) = Mariner IV (Alexander et al., 1965)
▶ (ref. 50) = Various Satellites (Nazarova, 1968)
▼ (ref. 51) = Lunar Explorer 35 (Alexander et al., 1971)
▽ (ref. 52) = Explorer XXIII (Naumann et al., 1969)
◁ (ref. 52) = Pegasus I, II, III (Naumann et al., 1969)
◇ (ref. 53) = Explorer XXIII (O'Neal, 1968)
◀ (ref. 54) = Cosmos 135 (Konstantinov et al., 1969)
◆ (ref. 55) = Cosmos 163 (Konstantinov et al., 1968)
△ (ref. 56) = Lunar Orbiter 1-5 (Gurtler and Grew, 1971)
(ref. 57) = NASA Model (Cour-Palais, 1974)
(ref. 58) = Hawkins, 1963 (photographic)
(ref. 59) = Moon, prehistoric flux (Neukum, 1973)
(ref. 59) = Moon, historic flux (Neukum, 1973)
(ref. 60) = (Radar) Kaiser, 1961
(ref. 61) = (Visual) Lindblad, 1967

Figure 13.—*Comparison of lunar and satellite micrometeoroid flux data.*

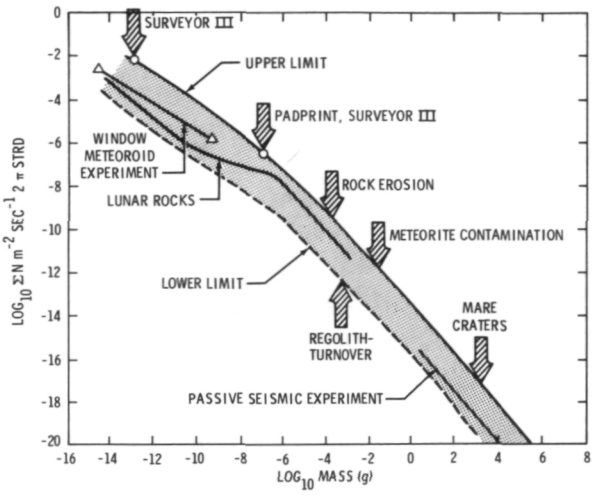

Figure 14.—*Constraints on the flux of micrometeoroids and larger objects, according to a variety of independent lunar studies.*

amount of meteoritic contamination in the lunar soil (ref. 66). Erosion rates on lunar rocks range from approximately .2 to 2 mm/10^6 years (refs. 67, 68, and 69). Taking the highest erosion rate and applying cratering data of Gault (ref. 28) make possible the definition of an upper flux limit. Furthermore, the negative findings on the Surveyor III camera lens (ref. 70) and the perfect preservation of the footpad print of Surveyor III (ref. 71) also define an upper limit. A lower limit results from the study of solar and galactic radiation tracks in lunar soils (refs. 72, 73, and 74). It is found that some cm-thick layers of regolith have resided on the lunar surface essentially undisturbed for ≈ 1 to 2×10^7 years. Because the regolith is believed to be reworked by micrometeoroids only, the flux could not have been significantly lower than indicated; otherwise still older residence times for the soil layers would be obtained. Strictly, only the passive seismometer, the Apollo windows, and the mare craters yield a cumulative mass distribution. All other parameters are a bulk measure of either meteoroid mass or energy; the corresponding "flux" was calculated using the differential mass distribution obtained from lunar microcraters. Accordingly, the corresponding arrows may be shifted anywhere along the line defining the "upper" and "lower" limits.

The data shown in figure 11 (ref. 75) suggest that the present flux is significantly higher than the average flux over the last 10^4 to 10^5 years (ref. 35). Gault et al. (ref. 34) and Morrison et al. (ref. 5) were the first to indicate such a possibility because absolute lunar rock exposure ages, erosion rates, and survival times of rocks appeared to be incompatible with computed values that were based on present-day meteorite fluxes derived from satellites. Neukum (ref. 59) expanded on these interpretations and his "historic" and "prehistoric" fluxes are incorporated in figure 13. Because the annealing behavior for radiation tracks during long-term exposure in the lunar environment is not well known and because all potential errors—both in the age dating as well as crater-counting—enter these considerations, a "historic" and "prehistoric" flux can only be tentatively proposed at present. The data of Hartung et al. (ref. 35) present the strongest evidence to date.

Although the magnitude of the flux may have varied over geological times, the mass-frequency distribution appears to have remained fairly constant. Frequencies measured on surfaces that were constituents of the soil (15927, 15301, 15001, and 60502) most likely do reflect the meteoroid bombardment that is older than that of most rocks. Their size-frequency distributions agree within the accuracy of measurement with "recent" crater populations.

Brownlee and Rajan (ref. 76) and Rajan et al. (ref. 77) discovered microcraters that are identical to lunar craters on the surface of glassy spherules, dislodged from the *interior* of the Kapoeta meteorite. This meteorite is a loosely consolidated microbreccia and a striking meteoritic analog to lunar soil breccias in many aspects. The formation age of Kapoeta is approximately 4×10^9 years (Rajan, personal communication, 1974). Within the counting accuracy, the size-frequency distribution of the Kapoeta microcraters is identical to lunar ones. Brownlee and Rajan furthermore dated one spherule

via solar flare tracks and derived a micrometeoroid flux that is within an order of magnitude of the present-day flux. Because the track retention over 4×10^9 years in glassy materials is poorly known, however, this exposure age and the resulting micrometeoroid flux has still larger uncertainties than young lunar glass surfaces. Blanford et al. (ref. 43) report numerous microcraters on feldspars separated from the very bottom (soil-sample 15001) of the 240-cm-long Apollo 15 drill core. The observed crater size-frequency distributions are essentially identical to those of rock samples 15205 and 15017 (see fig. 12). Because this soil was deposited at its site of collection more than 400 m.y. ago (ref. 78) the observed crater populations must have formed prior to that time. Micrometeoroid craters are also found in virtually every "soil-breccia" as well as genuine soil samples, though their actual geological time period of exposure is not known at present (ref. 24). Taking typical noble-gas exposure ages of lunar soils as statistically representative average values of the individual components, it may safely be concluded that micrometeoroid bombardment was active throughout geological time. From the presently available microcrater size-frequency distributions it also may be concluded that the mass-frequency distribution of micrometeoroids has not changed significantly if at all.

The studies on surfaces of old exposure ages demonstrate another unique characteristic of the "lunar rock micrometeoroid detector": it is principally possible to delineate the flux and potential variations thereof through geologic history. Such potential variations are of considerable interest to an explanation of the formation of the solar system for a variety of reasons:

1. The presence of a minimum micrometeoroid mass may be determined as a function of geologic time. This mass, in turn, may be used to calculate upper limits on the solar radiation pressure and thus to the luminosity of the Sun. Brownlee and Rajan (ref. 76) have attempted such calculations based on the minimum crater diameter observed on the Kapoeta materials and they concluded that the solar luminosity at $\approx 4 \times 10^9$ years was not higher than 1.7 times its present value.
2. The main source of micrometeoroids has to be sought in short-period comets. Significant variations in the flux of meteoroids may be related to short-period comet "activities," i.e., to an uneven, possibly sporadic rate of comet encounters that are capable of putting micrometeoroids with bound orbits into the inner solar system. In addition to these relatively short-term fluctuations (millions of years) it is also possible that the rate of comet injection into the inner solar system has undergone a long-term secular change due to a general depletion of the comet inventory.
3. Micrometeoroid detectors onboard Pioneer 8/9 have intercepted a non-negligible fraction of interplanetary particles that have hyperbolic orbits and thus are interpreted to be of interstellar origin (ref. 48). Thus lunar rocks offer a potential opportunity to study interstellar grains.

Most of the above possibilities, however, will require substantial amounts of work and are—at present—considered exciting challenges for future research. They are mentioned above only to stress the uniqueness and exciting potential of cratered lunar rock surfaces.

Lunar Regolith Dynamics

The lunar regolith is a layer of fragmental debris of variable thickness that lies upon fractured bedrock. Photogeologic investigations and detailed analysis of returned lunar materials revealed that repetitive meteoroid bombardment has been responsible for the formation of this layer to such an extent that other geological processes may be excluded. Impact cratering controls the overall growth of regolith; the lateral and vertical redistri-

bution of material; the downslope mass wasting; the mixing and degree of homogenization of individual layers; the erosion of lunar rocks; the evolution of regolith grain sizes; the formation of impact melts, agglutinates, and breccias; the migration of volatile elements; and the admixture of meteoritic components and other parameters that make up the physical, chemical, and petrographic characteristics of lunar "soils." As a consequence, it appears appropriate to combine observational lunar crater data and experimental impact crater mechanics into computational models to arrive at a theoretical understanding of these processes.

A variety of computational results concerning mass-movement, erosion rate of rocks, etc., are available (refs. 34, 59, 63, 79, and others). However, all these analyses suffer from the fact that they yielded only "average" values because the computations did not account for the vagarities of the random impact process. Models that do, however, account for the randomness of the impact process both in space and time have been developed recently and are described below. The models may be used to gain a qualitative if not quantitative insight into some of the above processes. Some of these models consider craters up to 1500 m in diameter and thus are of drastically different dimensions than the craters treated in the preceding sections. Furthermore, it is also important to note that the models are principally independent of the absolute flux of meteoroids. The time parameter is linearly related to the total number of craters produced. Thus model elapsed times can easily be converted into absolute times by applying the best estimate of the absolute meteoroid and micrometeoroid infall rates.

LARGE-SCALE REGOLITH CRATERING

The gross-accumulation of the regolith debris layer has been the subject of a variety of treatments, e.g., Marcus (ref. 80) and Shoemaker (ref. 63). It has been demonstrated that the overall regolith thickness increases with increasing numbers of craters that range roughly in diameter from 10 to 1000 m. Oberbeck and Quaide (ref. 81) pointed out that the growing debris layer acts as a buffering medium and thus strongly controls the geometry of different crater sizes. Accordingly, the actual thickness for a given lunar surface area can be related to the total number of craters produced as well as to the relative frequencies of differently shaped craters such as "normal," "flat-bottomed," "concentric," and "central mound" craters.

Oberbeck et al. (ref. 82) have developed a large-scale Monte Carlo-based computer program that simulates the evolution of the regolith and that also predicts the relative frequencies of the above four basic crater morphologies for any given regolith thickness. It is important to note that these calculations were performed with observed lunar cratering parameters, i.e., detailed crater geometries and distributions of associated ejecta blankets. No cratering scaling laws needed to be assumed.

A crater production size-frequency distribution of $N = KD^{-3.4}$ was empirically determined and used throughout these calculations (N = cumulative number of craters larger than diameter D, i.e., > 1 m). Some pertinent results are discussed below; for detailed information the reader is referred to Oberbeck et al. (ref. 82).

Figure 15 illustrates the relationship of the calculated median regolith thickness (R_m) as a function of absolute numbers of craters produced. A relationship of

$$R_m = 6.2 \times 10^{-5} K^{.64} \qquad (1)$$

is derived and may be used to predict the median thickness for any surface area where crater size-frequency distributions can be determined and where the cumulative crater production distribution has the form of $N = K \cdot D^{-3.4}$.

However, the regolith thickness is variable over distances measured in hundreds of meters as evidenced by high-resolution photography and field inspection by the astronauts, despite the fact that the overall reference surface must have been exposed to the meteoroid bombardment for the same period of time. Figure 16 compares actually measured

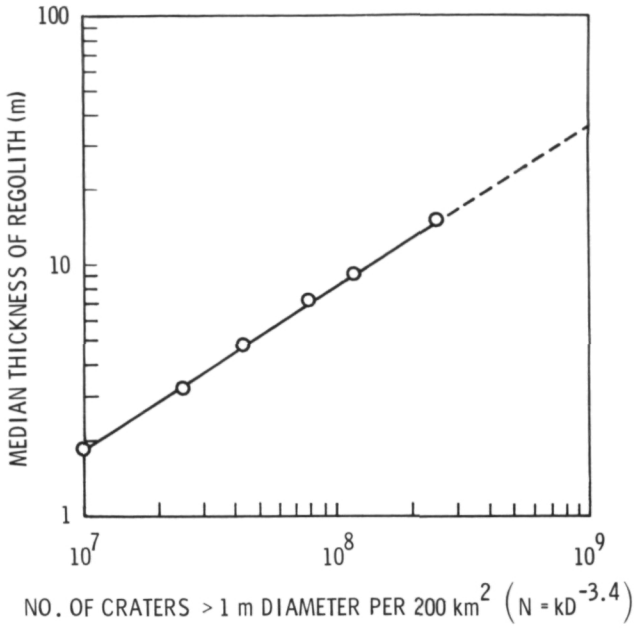

Figure 15.—*The overall regolith growth as a function of craters produced, i.e., time (see equation 1).*

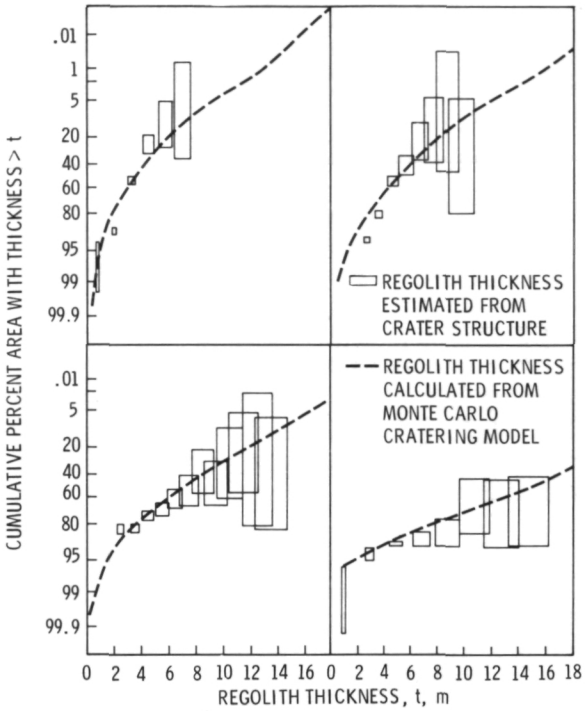

Figure 16.—*Empirically determined regolith thickness distribution for four different lunar surfaces measuring ≈ 200 km² each. The empirical determination is based on the abundance of various crater geometries reflecting the presence of a competent substrate. Note the good agreement between observations and Monte Carlo cratering simulations.*

thickness distributions (ref. 81) with those obtained in the Monte Carlo simulations. The agreement is good and lends additional support to the hypothesis that the regolith at the sites investigated by Quaide and Oberbeck (ref. 81) is primarily caused by impact comminution processes.

However, the above Monte Carlo model on regolith formation yielded additional information: with increasing thickness of regolith, only larger and larger craters are capable of penetrating the existing, buffering debris layer. Thus, with increasing time, it takes larger and larger craters to excavate pristine bedrock. The Monte Carlo simulations therefore continuously monitored, per each crater size class, the total volume excavated from the pristine substrate (V_s) and the already existing regolith layer (V_R) throughout the time required to build up the regolith to a given thickness. Figure 17 illustrates the ratio V_s/V_R for three different regolith depths. The ratio V_s/V_R is a function of crater diameter and is described by

$$V_s/V_R = C \cdot D^n \qquad (2)$$

where C is a constant for a given distribution of craters ($n = 1 - 1.3$); furthermore, C can be related to K in the crater distribution expression $N = KD^{-3.4}$ by

$$C = 1.02 \times 10^6 K^{-1.06} \qquad (3)$$

and by substitution

$$V_s/V_R = 1.02 \times 10^6 K^{-1.06} D^n \qquad (4)$$

Thus, over the range of values of K characteristic for mare terrains (as an example), the effective size boundary between mixing and new debris-producing craters becomes progressively larger. The average mixing zone therefore becomes deeper. Accordingly, older and thicker reolith deposits should be more thoroughly reworked than more youthful ones.

Figure 18 illustrates the cumulative contributions of various-sized craters that have built up a regolith layer of 4.7 m in median thickness. It is obvious from figures 17 and

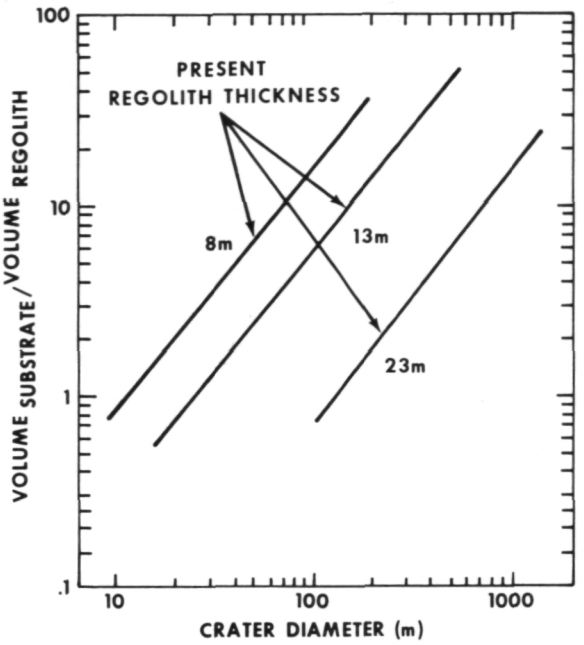

Figure 17.—*Relative contributions of pristine bedrock from the "substrate" for various crater sizes and regolith depths. The "volume regolith" is that volume that is reworked debris excavated by prior cratering. Note that predominantly the larger craters excavate bedrock and thus chiefly contribute to the overall regolith growth with increasing regolith thickness, i.e., time.*

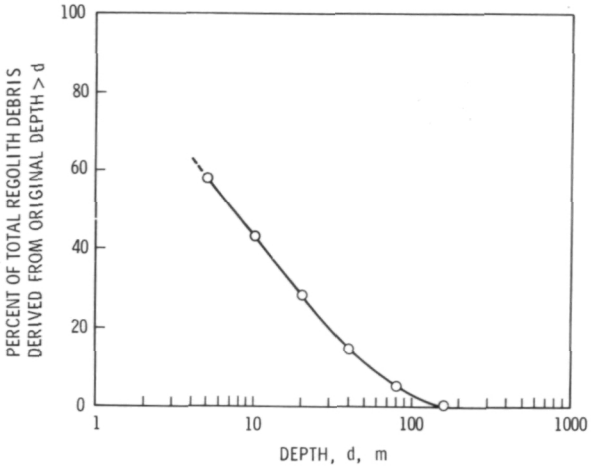

Figure 18.—*Contributions (= volume percent) of various source areas at depth "d" to the overall composition of a typical mare regolith having a median thickness of 4.7 m.*

18 that relatively small craters (e.g., < 10 m in diameter) have contributed significant amounts to the overall regolith, but it is also readily seen that these contributions occurred while the regolith was relatively thin, i.e., in the early stages of regolith formation. At present it is predominantly structures > 100 m in diameter that control the overall regolith growth while the smaller structures are confined to reworking these materials. As a consequence, the regolith thickness increases in general and in particular during its more recent history (i.e., the past $\approx 10^9$ years) due to the effects of relatively large cratering events that are capable of excavating pristine bedrock. This newly added material will always be delivered on top of the existing debris in discrete swaths of ejecta. The regolith therefore has to be envisioned as a complex sequence of numerous, overlapping ejecta blankets. These discreet blankets constitute some first-order discontinuities and heterogeneities in the evolving regolith. We will demonstrate in the next chapter that it is principally possible to preserve parts of these blankets despite heavy meteorite bombardment. Though there will be extensive mixing, there will not be complete homogenization of the regolith.

SMALL-SCALE REGOLITH CRATERING

It is obvious from the preserved stratigraphy in returned core tube samples that reworking has not obliterated all stratification in the regolith. It is just as obvious, however, that every stratum that resided at the very lunar surface has been subjected to the meteoroid bombardment and the reworking process which—due to the mass-frequency distribution of interplanetary matter—does operate on a micron-to-meter scale. The extent to which a stratum survives thus must be a function of its original thickness and length of surface residence time before it is blanketed by ejecta of sufficient thickness to effectively remove it from the active zone of reworking. Absolute parame-

ters for these variables principally vary with absolute time; i.e., the cumulative number of craters produced. The absolute number of craters that contributed to the history of returned samples must certainly be larger than the numbers presently observable in the respective sampling areas because these are in crater-saturation for craters < 100m in diameter (refs. 22 and 63). Thus the potential surface history of sampled materials can be understood only if a continuous bombardment history is assumed in computational models.

Because meteoritic impact is a random process, any given point on the lunar surface has a unique history as compared with any other given point. On the other hand, the dominant role of meteoroid impact suggests that over extended periods of time any two areas of a given size will have experienced similar histories that differ only in details to a greater or lesser degree. Thus computational analyses that yield "average" values may be useful in understanding the basic processes. However, they should be applied only with extreme caution to actual sample data because of the uniqueness of each individual sampling location. "Averages" are certainly a valid framework for returned sample interpretations; but they should be applied only if sufficient statistical sample data are available. For any *individual* data point such averages cannot be applied and may lead to grossly erroneous results, because significant deviations from the "average" have to be expected from a random process.

Gault et al. (ref. 83) have shown that the probability P_u of a given point on the lunar surface remaining undisturbed, i.e., lying outside a crater of apparent diameter D in a time interval t is given by

$$P_u = \exp.\ (-\pi NtD^2/4) \qquad (5)$$

where N is the flux of the randomly distributed impacting bodies per unit time and area which produce craters of diameter D. The probability P_c of a given point's having been affected, i.e., lying within exactly n craters of size D can be expressed as

$$P_{c(n)} = P_u(\pi NtD^2/4)^n/_n(!) \qquad (6)$$

Equation 6 is the Poisson probability function. Using the values given by Molina (ref. 84) for a range of $n = 0 - 153$ and $(\pi NtD^2/4) = .001 - 100$ and calculating additional terms up to $n = 10^6$, Gault et al. (ref. 83) calculated how many times a given surface area may be impacted. A microme-

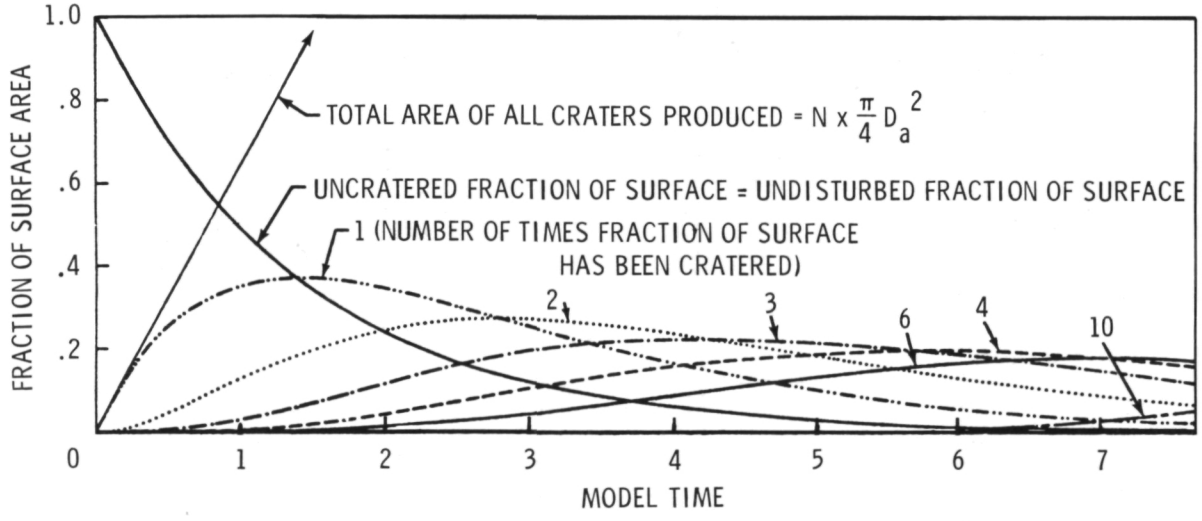

Figure 19.—*Analytical model based on Poisson probability function describing the amount of surface area (percent) that will be affected by meteoriod impact, and the number of times impact will have occurred after given model elapsed times.*

teoroid mass-distribution of the form $N = 1.45\ m^{0.47}$ was used for 10^{-13} to 10^{-7}g meteoroid mass (m) and $N = 9.14 \times 10^{-6} m^{1.213}$ for projectiles 10^{-7} to 10^{3} g. Furthermore a standard impact velocity of 20 km/s, together with laboratory cratering data into unconsolidated materials (ref. 28), was applied in these calculations. The principal result is shown in figure 19.

Virtually identical results (fig. 20) were obtained in a Monte Carlo-based computer-simulation by Hörz et al. (ref. 85), that applied the crater size-frequencies of figure 6 and a random number generator to determine impact coordinates and the magnitude of each cratering event. The curve labeled "1x" in figure 20 indicates how much surface area is affected at least one time. Note that 50 percent of the test surface (= 44 cm²) is already cratered after 8300 craters, 152 to 22500 μm in spall diameter. It takes more than a factor of 10 additional craters to affect the remaining 50 percent. Though qualitatively not surprising, these absolute numbers were unexpected. Furthermore, figure 20, for example, illustrates that by the time 99 percent of the surface is cratered at least 1 × (99 percent probability), 92 percent of the surface is already cratered twice, 81 percent has suffered at least three impacts, 59 percent is cratered four times, etc. As 99.99 percent of the surface is cratered at least once, 88 percent will already be affected at least five times, etc.

An extension of the data illustrated in figure 20 is presented in figure 21, which is based on 10^6 craters (ref. 85). Per each model-elapsed time, it was determined how often a given fractional surface area was impacted. Note that when the entire area (= 100 percent) is cratered at least one time, 50 percent has suffered already 12 impacts and 10 percent surface was cratered at least 17 times. Or, alternatively, if it takes one time to affect 50 percent of a lunar surface, it will take 3.8 times longer to affect 90 percent, a factor of 6.6 longer to cover 99 per-

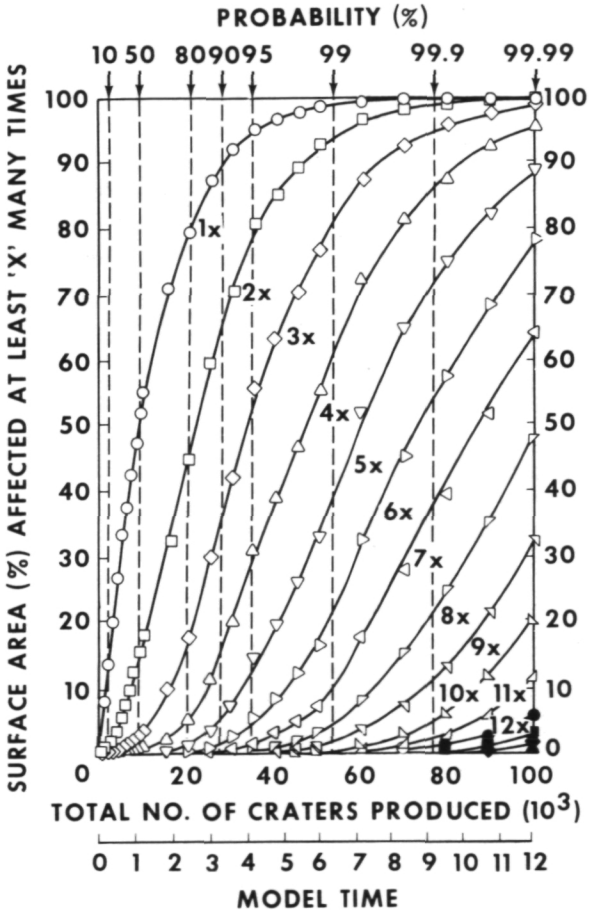

Figure 20.—*Almost identical data as in figure 19, resulting from a Monte Carlo computer program. Note the multiple bombardment history of fractional surface areas with increasing time, i.e., 10^5 craters produced.*

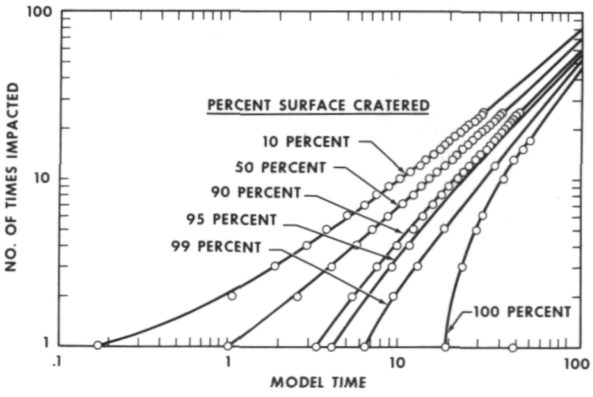

Figure 21.—*General probability of multiple bombardment history for various fractional surface areas (total craters produced: 10^6; see text).*

cent and, finally, 19 times longer to crater 100 percent of the surface. The model times indicated in figures 19 through 21 will be used in identical fashion throughout this report. Unit time is defined as the time required to affect 50 percent of the surface area at least one time.

Figures 19 through 21 illustrate a fundamental characteristic of the impact process. While finite—though admittedly small—surface areas may remain unaffected for long time periods, other areas have already suffered repetitive bombardment. Consequently, within any cratered terrain, small surface areas may be encountered that have dramatically different bombardment histories despite the fact that they were exposed to the same micrometeoroid environment for the same period of time.

We now turn to the mixing of the regolith. The above models are also a measure of how much kinetic energy is deposited randomly in space and time into a unit area of lunar surface. Therefore, one can associate with that energy either a crater diameter (as above) or a corresponding crater depth. Gault et al (ref. 83) applied these concepts using the meteoroid mass distribution and the probability theory given above together with cratering mechanics of Gault (ref. 28). The number of impacts per unit area (e.g., fig. 21) were converted into "depth excavated" because each crater diameter may be associated with a given crater depth. Results of such calculations are illustrated in figure 22. The absolute timescale is based on the Gault et al. micrometeoroid flux (ref. 34), assumed to be constant over geological times. Though these absolute rates of regolith turnover are considered realistic for about the past 10^8 to 10^9 years, they are certainly not valid for periods $> 10^9$ years. Gault et al. (ref. 83) therefore also calculated the same data for a time variable flux; these data are shown in figure 23.

The principal result of figures 21 and 23 is of course the high turnover rate of the regolith surface itself, e.g., figure 22: while it takes approximately 10^7 years to completely turn over an 8-mm-deep zone at least once, the uppermost mm of the very same area has been turned over already 25(!) times; or when 99 percent of an 8-mm-deep layer is turned over at least once, 50 percent of the same surface will have already been turned over to a 1.4-cm depth. As a consequence, there exists a very thin surface zone, approximately 1 mm in thickness, in which extreme mixing and homogenization of components occurs. However, the lunar regolith becomes relatively quiescent rather quickly

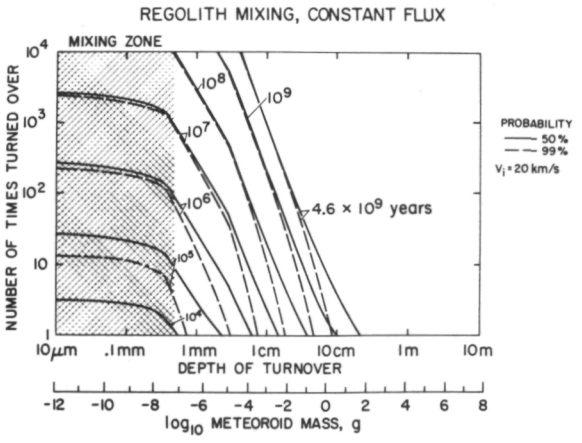

Figure 22.—*The detailed turnover history of various regolith depths, as a function of absolute time and a constant flux.*

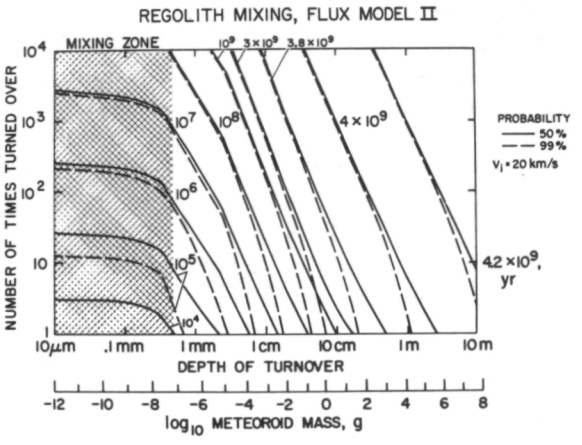

Figure 23.—*Same as figure 22, but with use of a meteoroid model flux that increases with geologic time to match the observed crater densities at the Apollo 12 landing site.*

with depth; e.g., even with a meteoroid flux that accounts for an increase in bombardment (fig. 23) in early lunar history (=2 to 3.8×10^9 years), a 1-m-thick layer is turned over only once with 99 percent confidence. This accounts for the observation of Russ et al. (ref. 78) that a major section of the Apollo 15 deep drill core had been residing completely undisturbed on the lunar surface for the past 500 m.y. We therefore conclude that due to the mass-frequency distribution of interplanetary matter that is vastly dominated by relative small particles in the 10^{-8} to 10^{-4} g mass range, only an upper mm is thoroughly mixed before an adjacent larger impact event covers the area and effectively removes the mixing layer from the active reworking zone. It is thus possible to preserve the observed small-scale stratigraphy in the regolith.

However, though each surface layer undoubtedly has its peculiar surface history, it is not correct to conclude that each layer was *deposited* at the eventual site of recovery by *one* discrete impact event. Gault et al. (ref. 86) and Stöffler et al. (ref. 87) demonstrated that the ejecta blankets of experimental impact craters in layered quartzsand targets have part of the original target-stratigraphy preserved, though in reversed sequence, i.e., overturned. Similar observations are also made around large-scale nuclear and chemical explosion craters as well as terrestrial impact craters (e.g., the 25-km-diameter Reis-structure, Germany (ref. 88). As a consequence, each regolith crater on the Moon will preserve—though certainly in a somewhat degraded fashion—the original stratigraphic section. Therefore a variety of discrete layers may be excavated and redeposited at the site of recovery by a large single impact regardless of whether they had drastically different exposure histories before this *last* depositional episode.

Furthermore, processes other than direct deposition of impact ejecta blankets may also cause an apparent layering in the recovered regolith cores. For example: small-scale slumping on the walls of regolith craters may be a significant process. It can also be envisioned that soft soil breccias ejected by a larger event completely desintegrate upon landing at significant distances from the primary crater. Rocks that survived such a landing at the end of a ballistic trajectory are subject to micrometeoroid erosion and their erosion products may be foreign to the new environment, thus causing a local "heterogeneity" and therefore a "layer" in the regolith stratigraphy. Virtually nothing is known about the lateral dimensions of the regolith "layers" and it is possible that their areal extent is rather limited. Beyond any doubt, however, caution is necessary to postulate that each observed layer was last deposited by one discrete impact event; such interpretations may be grossly in error.

LUNAR ROCK EROSION

Studies of the grain size distribution of individual cratering experiments (refs. 31 and 89) revealed that the ejecta of one given event are significantly more coarse-grained than grain sizes reported from the lunar regolith (e.g., refs. 90 and 91). Thus larger regolith components must be broken up, i.e, "eroded," by small-scale cratering events. The visual inspection of lunar rocks both on lunar surface photographs and in the laboratory reveals that micrometeoroid impact causes erosion and eventual destruction of rock specimens exposed to space. The micrometeoroid complex operates on two different scales and accordingly results in two significantly different effects, i.e., "single particle abrasion" and "catastrophic rupture" (refs. 34, 59, 63, 79, and others).

"Single particle abrasion" is caused by relatively small craters, as compared with the overall size of a specific rock, and it results in an effect similar to sandblasting. It is largely responsible for gradual mass wasting associated with a general rounding of the rocks (fig. 24). In contrast, "catastrophic rupture" is accomplished only by craters of relatively large size with respect to a given rock mass, i.e., only by impacts of sufficient energy to generate penetrative fracture systems (fig. 25).

Hörz et al. (ref. 16) simulated the "single particle abrasion" process via Monte Carlo-based computer models; up to 10^6 craters 152 to 25 000 μm in spall diameter were produced on a 25-cm^2 surface area. Figure 26 displays some computer-generated profiles after a variety of crater numbers produced. Figure 27 illustrates the average erosion depth as a function of time. Note the influence of a few, though large, events in particular in figure 27, but also in figure 26. Applying a best estimate for the absolute micrometeoroid flux averaged over the past 10^6 years, Hörz et al. (ref. 85) arrive at erosion rates for crystalline lunar rocks of .3 to .6 mm per 10^6 years. The erosion rate for breccias may be higher, because of less compressive target strength (ref. 34).

Figure 28 illustrates an additional result of the above Monte Carlo simulation relating to the "representative" nature of finite size rock chips available in the laboratory to delineate lunar surface processes. The computer iterated over the entire test surface and searched for the least (=shallowest) and most eroded (=deepest) "unit areas" that were defined as 5, 2, 1, .64, and .16 cm^2. The "extremes" in erosional state are compared with the average of the entire area in figure 27. The deviation from the average is a direct measure of how typical or atypical small lunar rock chips may be with respect to their parent rock. The deviations observed are considerable and constitute ample evidence that the random nature of the impact process has to be seriously considered in the analysis of discrete, finite-size rock chips. Unless it is demonstrated otherwise, that such a sample is truly "representative" of the parent rock, the results obtained may

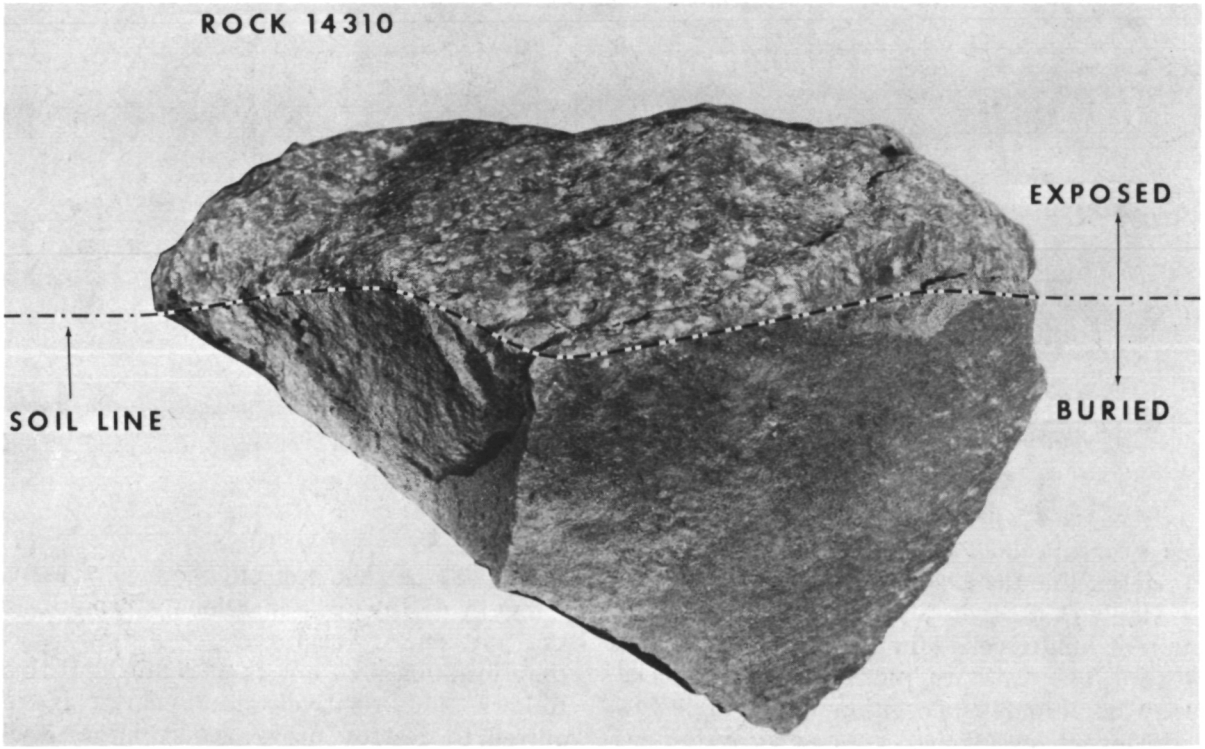

Figure 24.—*Typical lunar rock (14310) illustrating the effects of single particle abrasion. As indicated by the soil line, parts of this rock were buried in the lunar regolith. The buried portion is characterized by sharp, angular fracture surfaces. In contrast, the surfaces exposed to the micrometeoroid bombardment are abraded and significantly rounded.*

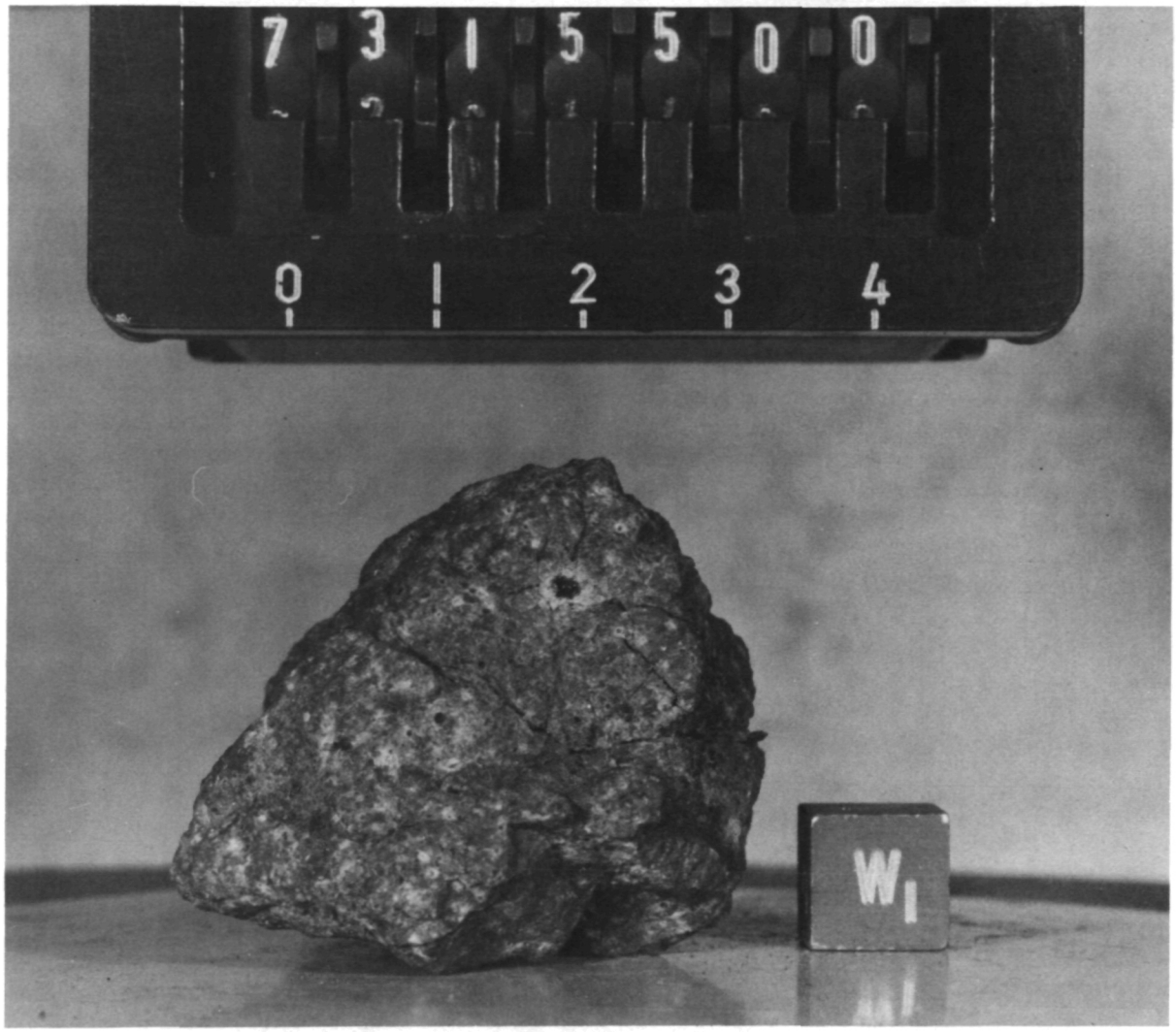

Figure 25.—*Lunar rock 73155 that has suffered an exceptionally large impact almost capable of catastrophically rupturing the entire hand specimen.*

only be used with caution to delineate "averages," e.g., solar flare particle track densities to determine the absolute exposure age.

Gault et al. (ref. 34) treated the destruction of lunar rocks due to "catastrophic rupture." The catastrophic breakup of rocks may be accomplished either by a single impact event of sufficient energy or by the cumulative effects of a number of smaller impacts; the rupture energy (E_R) is cumulative (ref. 92). The energy required to rupture a rock ($\cong$ sperical body) of radius r can be described as

$$E_R = 2.5 \times 10^6 \, S_c \, r^{-0.225} \qquad (7)$$

where S_c is the unconfined compressive strength of the rock in kilobars; and E_R is the unit energy required *per gram,* rather than total mass, of a rock of radius r. It thus follows that relatively less energy is required to destroy progressively larger rock specimens. Figure 29 compares actual measurements of the very largest pit craters observed on lunar rocks and the relations expressed by equation (7). The agreement is

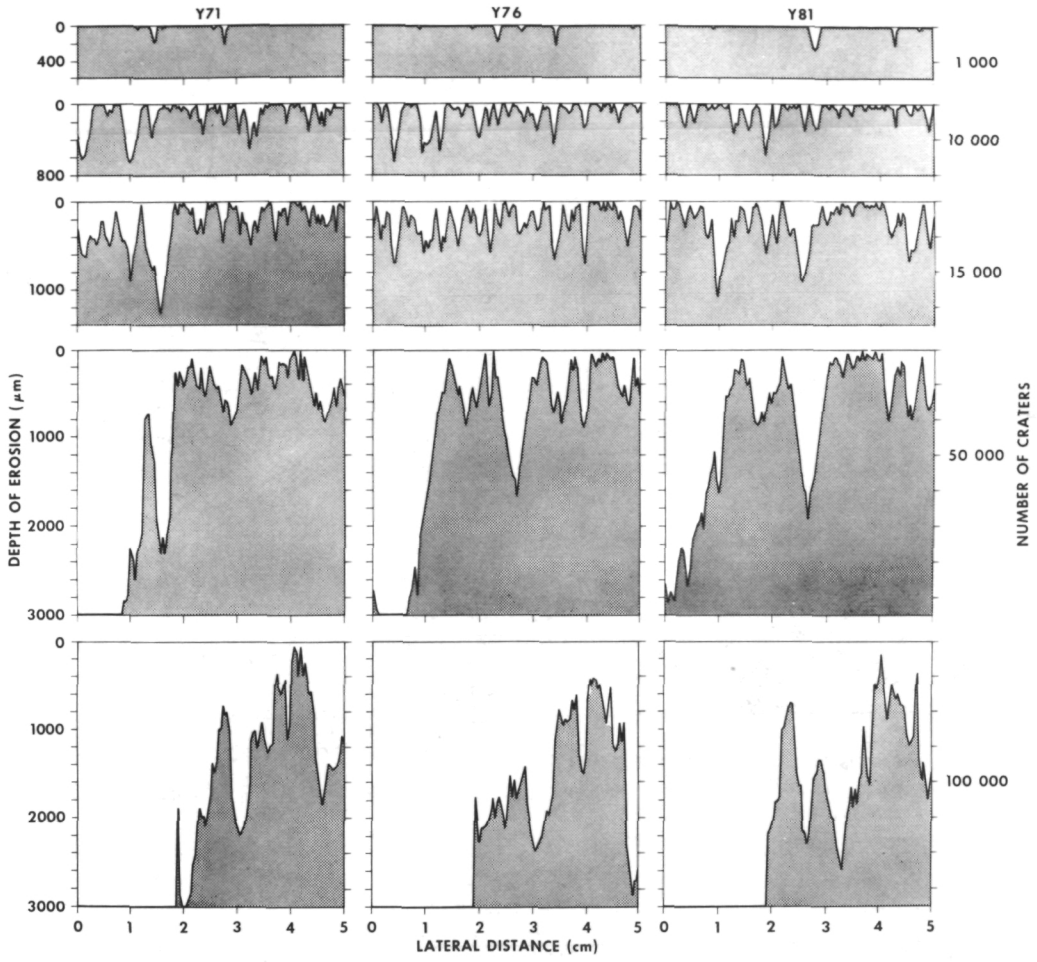

Figure 26.—*Computer-generated erosion profiles of a lunar rock. According to each number of total craters produced, profiles taken at three different localities (Y_{71}, Y_{76}, Y_{81}) are illustrated (white—volume eroded; stippled—remaining rock; the vertical exaggeration is 17 times).*

good (ref. 26). Figure 29 illustrates the mean survival time before catastrophic rupture occurs for various hypothetical rock material, considering compressive strength and rock mass as the main variables (ref. 34).

When the results of "single particle abrasion" and "catastrophic breakup" are combined, the following conclusions emerge: while, for example, a 1-kg rock will survive catastrophic desintegration for about 3×10^6 years, it has suffered in the meantime "single particle abrasion" that effectively removed a surface layer of only about 1 to 2 mm in thickness. (See figure 30). Thus "catastrophic rupture" must be considered the vastly superior process in obliterating lunar rocks. "Single particle abrasion" plays a minor role only, but it is still an order of magnitude more effective than sputtering processes caused by high energetic radiation (ref. 79) 1973.

Conclusions

The authors hope their efforts have demonstrated that the study of lunar microcraters has significantly contributed to our present understanding of the micrometeoroid complex:

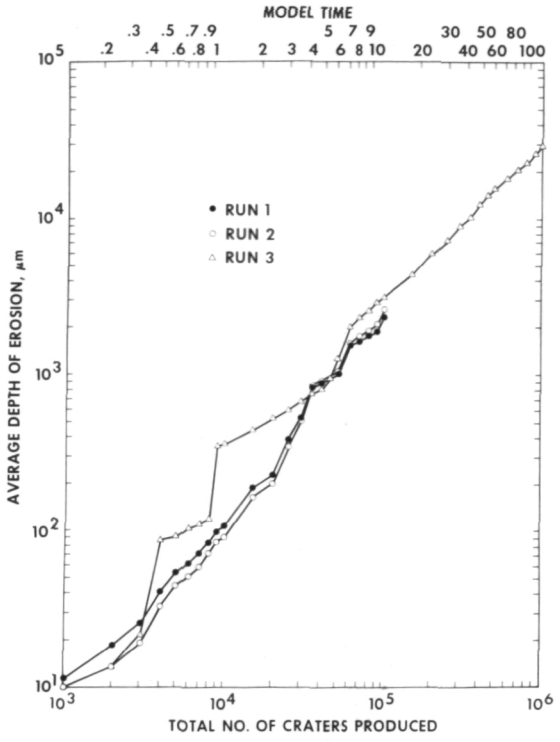

Figure 27.—*Average erosion depth resulting from a Monte Carlo computer simulation. The best estimate for erosion is based on 10^6 craters, i.e., run 3. Notice the influence of some few—however, very large—craters.*

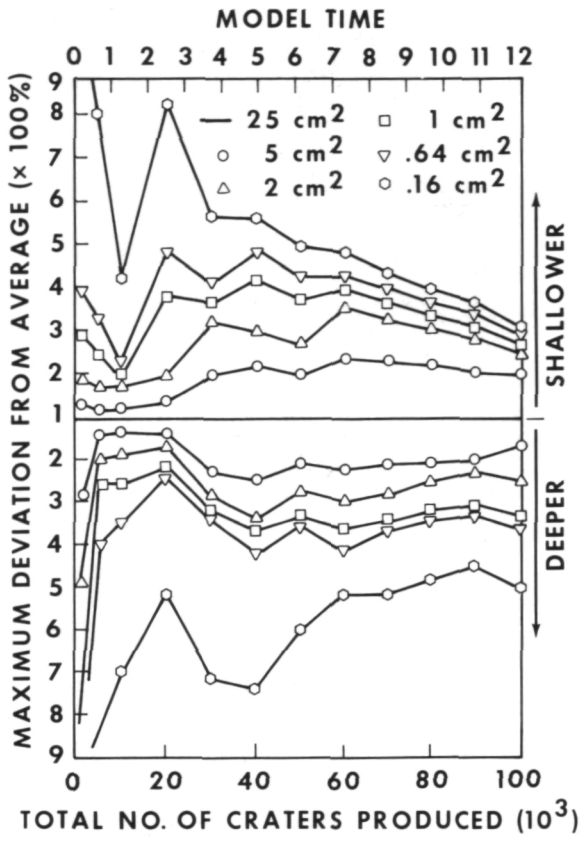

Figure 28.—*Extremes in deviation of erosional state of various, absolute surface areas (5, 2, 1., .64, and .16 cm²) compared with the average of a 25 cm² surface.*

1. Contrary to popular astronomical hypotheses, the micrometeoroids have densities from 2 to 4 g/cm³. They are also equant if not spherical in shape; forms like needles, whiskers, platelets, rods, etc., may safely be excluded.
2. The mass-frequencies from 10^{-12} to 10^{-3} g are in agreement with previous meteoroid data. However, particle masses as small as 10^{-15} g are responsible for the formation of microcraters $< .1$ μm in diameter. This result negates the existence of the celebrated "radiation pressure cutoff" at particle masses $< 10^{-12}$ g.
3. The average micrometeoroid flux for the past 10^6 years could be established within a factor of 5. In agreement with satellite measurements, it is likely that the present micrometeoroid activity is about an order of magnitude higher than this long-term average.
4. Though absolute flux data do not exist at the moment, there is ample evidence that the micrometeoroid complex existed throughout geological time.
5. The potential of the "lunar micrometeoroid detector" is not fully exhausted at the moment.

The micrometeoroid complex and larger meteoroids are primarily responsible for the evolution and physical-chemical makeup of the lunar regolith; they effectively control the overall regolith growth as well as small-scale stratigraphy. The regolith has to be envisioned as a complex sequence of ejecta blankets that have not necessarily lost their integrity. The mixing, "gardening," and

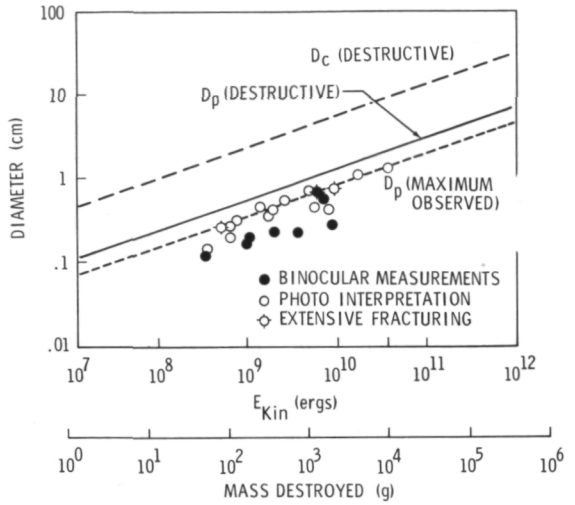

Figure 29.—*Spall and pit diameters required for catastrophic rupture of a given rock mass, according to calculations based on experimental and observational results. Diameter,* D_p *(destructive) is considered an upper limit for pit diameters observable on lunar rocks;* D_c *is an experimental limit referring to the crater diameter, i.e., spall diameter* (D_s). *Ratios for* D_s/D_p *in lunar rocks are typically from 3.8 to 4.6. The agreement of observations on lunar rocks with those on experimental rupture is excellent.*

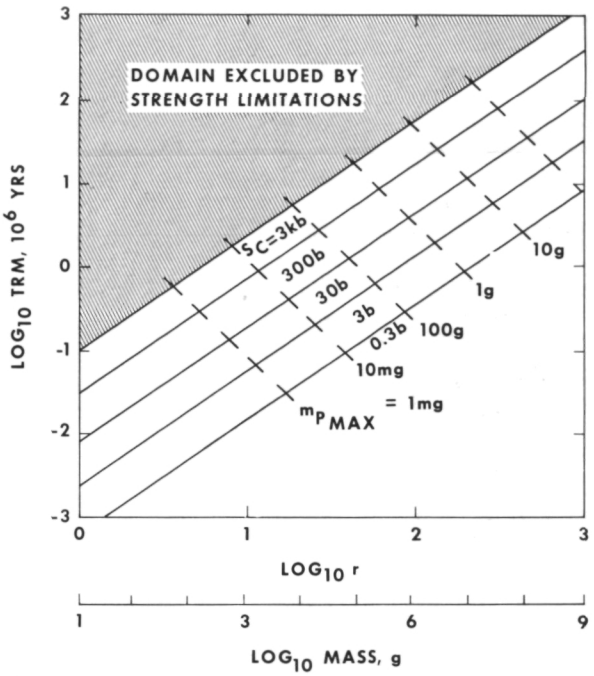

Figure 30.—*Calculated mean residence time before destruction by catastrophic rupture for spherical rocks of radius* r *and compressive strengths* (S_c), *exposed to the micrometeoroid bombardment. Masses of the largest particles* (M_{pmax}) *contributing to the rupture process are indicated.*

homogenization are largely confined to the uppermost layer of approximately 1-mm thickness. Lunar rocks are effectively destroyed by micrometeoroids, with the "catastrophic rupture" process dominating the "single particle abrasion." These results will aid not only in the interpretation of lunar materials but also in that of other planetary surfaces as well.

References

1. Shoemaker, E. M., R. M. Batson, H. E. Holt, E. C. Morris, J. J. Rennilson, and E. A. Whitaker, Observations of the Lunar Regolith and the Earth From the Television Camera on Surveyor 7. *J. Geophys. Res.*, Vol. 74, 1969, pp. 6081–6119.
2. Bloch, M. R., H. Fechtig, W. Gentner, G. Neukum, and E. Schneider, Meteorite Impact Craters, Crater Simulations, and the Meteoroid Flux in the Early Solar System. *Proc. Second Lunar Science Conference, Geochimica et Cosmochimica Acta*, Supplement 2, Vol. 3, 1971, pp. 2639–2652.
3. Hartung, J. B., F. Hörz, and D. E. Gault, Lunar Microcraters and Interplanetary Dust. *Proc. Third Lunar Science Conference, Geochimica et Cosmochimica Acta*, Supplement 3, Vol. 3, 1972, pp. 2735–2753.
4. Hartung, J. B., F. Hörz, and D. E. Gault, Lunar Rocks as Meteoroid Detectors. In *Proc. Internal Astron. Union Colloq.* No. 13, The Evolutionary and Physical Problems of Meteoroids, in press, 1972.
5. Morrison, D. A., D. S. McKay, and H. J. Moore, Microcraters on Apollo 15 and 16 Rocks. *Proc. Fourth Lunar Science Conference, Geochimica et Cosmochimica Acta*, Supplement 4, Vol 3, 1973, pp. 3235–3253.
6. Vedder, J. F., Microcraters in Glass and Minerals. *Earth Planet. Sci. Letters*, Vol. 11, 1971, pp. 291–296.
7. Vedder, J. F., Craters Formed in Mineral Dust by Hypervelocity Microparticles. *J. Geophys. Res.*, Vol. 77, 1972, pp. 4304–4309.
8. Fechtig, H., J. B. Hartung, K. Nagel, and G. Neukum, Microcrater Studies, Derived Me-

teoroid Fluxes and Comparison With Satellite Borne Experiments. *Lunar Science*, Vol. V, Lunar Science Institute, Houston, 1974, pp. 222–224; also in *Proc. Fifth Lunar Science Conference*.

9. MANDEVILLE, J. C., AND J. F. VEDDER, Microcraters Formed in Glass by Low Density Projectiles. *Earth Planet. Sci. Letters*, Vol. 11, 1971, pp. 297–306.
10. NEUKUM, G., *Untersuchungen über Einschlagskrater auf dem Mond.* Doctor's Thesis, University of Heidelberg, 1971.
11. SCHNEIDER, E., *Mikrokrater auf Mondgestein und deren Laborsimulation.* Ph.D. Thesis, Heidelberg, Germany, unpublished, 1972.
12. VEDDER, J. F., AND J. C. MANDEVILLE, Microcraters Formed in Glasses by Projectiles of Various Densities. *J. Geophys. Res.*, in press, 1974.
13. MANDEVILLE, J. C., *Etude de Crateres Formes sur des Surfaces de Verre par L'Impact de Micrometeorides Artificelles.* Ph.D Thesis, No. 1334, Toulouse, France, unpublished, 1972.
14. KERRIDGE, J. F., AND J. F. VEDDER, Accretionary Process in the Early Solar System: An Experimental Approach. *Science*, Vol. 177, 1972, pp. 161–162.
15. BROWNLEE, D. E., F. HÖRZ, J. F. VEDDER, D. E. GAULT, AND J. B. HARTUNG, Some Physical Properties of Micrometeoroids. *Proc. Fourth Lunar Science Conference, Geochimica et Cosmochimica Acta*, Supplement 4, Vol. 3, 1973, pp. 3197–3212.
16. HÖRZ, F., D. E. BROWNLEE, H. FECHTIG, J. B. HARTUNG, D. A. MORRISON, G. NEUKUM, E. SCHNEIDER, AND J. F. VEDDER, Lunar Microcraters and Their Implications for the Micrometeoroid Complex. *Planet. Space Sci.*, Vol. 23, 1975, pp. 151–172.
17. VEDDER, J. F., AND H. LEM, Profiling With the Electron Microscope. *Photogrammetric Engr.*, Vol. 38, 1972, pp. 243–244.
18. CARTER, J. L., AND D. S. MCKAY, Influence of Target Temperature on Crater Morphology and Implications on the Origin of Craters on Lunar Glass Spheres. *Proc. Second Lunar Science Conference, Geochimica et Cosmochimica Acta*, Supplement 2, Vol. 3, 1971, pp. 2653–2670.
19. HARTUNG, J. B., AND F. HÖRZ, Microcraters on Lunar Rocks. *Proc. 25th Int. Geol. Cong.*, Montreal, Section 15, Planetology, 1972, pp. 48–56.
20. VERNIANI, F., Structure and Fragmentation of Meteoroids. *Space Sci. Res. Rev.*, Vol. 10, 1969, pp. 230–261.
21. HUGHES, D. W., Interplanetary Dust and Its Influx to the Earth's Surface. *Space Res.*, Vol. XIV, COSPAR 73, Konstanz, Germany, in press, 1973.
22. GAULT, D. E., Saturation and Equilibrium Conditions for Impact Cratering on the Lunar Surface: Criteria and Implications. *Radio Sci.*, Vol. 5, 1970, pp. 273–291.
23. NEUKUM, G., F. HÖRZ, D. A. MORRISON, AND J. B. HARTUNG, Crater Population on Lunar Rocks. *Proc. Fourth Science Conference, Geochimica et Cosmochimica Acta*, Supplement 4, Vol. 3, 1973, pp. 3255–3276.
24. SCHNEIDER, E., D. STORZER, A. MEHL, J. B. HARTUNG, H. FECHTIG, AND W. GENTER, Microcraters on Apollo 15 and 16 Samples and Corresponding Cosmic Dust Fluxes. *Proc. Fourth Lunar Science Conference, Geochimica et Cosmochimia Acta*, Supplement 4, Vol. 3, 1973, pp. 3277–3290.
25. HÖRZ, F., J. B. HARTUNG, AND D. E. GAULT, Micrometeorite Craters on Lunar Rock Surfaces. *J. Geophys. Res.*, Vol. 76, 1971, pp. 5770–5798.
26. HARTUNG, J. B., F. HÖRZ, K. F. AITKEN, D. E. GAULT, AND D. E. BROWNLEE, The Development of Microcrater Populations on Lunar Rocks, *Proc. Fourth Lunar Science Conference, Geochimica et Cosmochimica Acta*, Supplement 4, Vol. 3, 1973, pp. 3213–3234.
27. SCHNEIDER, E., AND F. HÖRZ, Microcrater Populations on Apollo 17 Rocks. *Icarus*, in press, 1974.
28. GAULT, D. E., Displaced Mass, Depth, Diameter and Effects of Oblique Trajectories for Impact Craters Formed in Dense Crystalline Rocks. *The Moon*, Vol. 6, 1973, pp. 32-44.
29. NAGEL, K., *Experiments zur Kratersimulation.* Master's Thesis, University of Heidelberg, Germany, unpublished, 1973.
30. NEUKUM, G., E. SCHNEIDER, A. MEHL, D. STORZER, G. A. WAGNER, H. FECHTIG, AND M. R. BLOCH, Lunar Craters and Exposure Ages Derived From Crater Statistics and Solar Flare Tracks. *Proc. Third Lunar Science Conference, Geochimica et Cosmochimica Acta*, Supplement 3, Vol. 3, 1972. pp. 2793–2810.
31. MOORE, H. J., D. E. GAULT, AND E. D. HEITOWIT, *Change of Effective Target Strength With Increasing Size of Hypervelocity Impact Craters.* Seventh Hypervelocity Impact Symposium, Tampa, Flordia, Nov. 17–19, Vol. 4, 1965, p. 341.
32. MILLMANN, P., The Observational Evidence for Mass Distribution in the Meteoritic Complex. *The Moon*, Vol. 8, 1973, p. 228.
33. DOHNANYI, J. S., Interplanetary Objects in Review: Statistics of Their Masses and Dynamics. *Icarus*, Vol. 17, 1972, pp. 1–48.
34. GAULT, D. E., F. HÖRZ, AND J. B. HARTUNG, Effects of Microcratering on the Lunar Surface. *Proc. Third Lunar Science Conference, Geochimica et Cosmochimica Acta*, Supplement 3, Vol. 3, 1972, pp. 2713–2734.
35. HARTUNG, J. B., D. STORZER, AND F. HÖRZ, To-

ward a Lunar Microcrater Clock. *Lunar Science*, Vol. V, Lunar Science Institute, Houston, 1974, pp. 307–309; also in *Proc. Fifth Lunar Science Conference*.

36. ZOOK, H., AND O. E. BERG, A Source for Hyperbolic Cosmic Dust Particles. *Planet. Space Sci.* in press, 1974.
37. JEDWAB, J., La Magnetite de le Meteorite D'Orgueil, Vue au Microscope Electronique a Balayage. *Icarus*, Vol. 15, 1971, pp. 319–340.
38. KERRIDGE, J. F., Low-Temperature Minerals From the Fine-Grained Matrix of Some Carbonaceous Meteorites. *Ann. New York Academy of Sciences*, Vol. 119, 1964, pp. 41–53.
39. DONN, B., The Origin and Nature of Solid Particles in Space. *Ann. New York Academy of Sciences*, Vol. 119, 1694, pp. 5–16.
40. ARRHENIUS, G., AND H. ALFVÉN, Asteroidal Theories and Experiments. *Physical Studies of Minor Planets, Proc. 12th Coll. Int. Astr. Union*, Tucson, Ariz., 1971, pp. 213–233.
41. GROSSMAN, L., Condensation in the Primitive Solar Nebula. *Geochimica et Cosmochimica Acta*, Vol. 36, 1972, pp. 597–619.
42. HARWIT, M., Origins of the Zodiacal Dust Cloud. *J. Geophys. Res.*, Vol. 68, 1963, pp. 2171–2180.
43. BLANFORD, G., D. S., MCKAY, AND D. A. MORRISON, Accretionary Particles and Microcraters. *Lunar Science*, Vol. V, Lunar Science Institute, Houston, 1974, pp. 67–68; also in *Proc. Fifth Lunar Science Conference*.
44. GINDILIS, L. M., N. B. DIVARI, AND L. V. REZNOVA, Solar Radiation Pressure on Particles of Interplanetary Dust. *Soviet Astron., A.J.*, Vol. 13, 1969, pp. 114–119.
45. NILSSON, C. S., F. W. WRIGHT, AND D. WILSON, Attempts to Measure Micrometeoroid Flux on the OGO II and OGO IV Satellites. *J. Geophys. Res.*, Vol. 74, 1969, pp. 5268–5276.
46. ALEXANDER, W. N., C. W. ARTHUR, J. L. BOHN, J. H. JOHNSON, AND B. J. FARMER, Lunar Explorer 35: 1970 Dust Particle Data and Shower-Related Picogram Ejecta Orbits. *Space Res.*, Vol. 12, 1972, pp. 349–355.
47. HOFFMAN, H. J., H. FECHTIG, E. GRÜN, AND J. KISSEL, First Results of the Micrometeoroid Experiment S 215 on the HEOS 2 Satellite. *COSPAR 1973*, Konstanz, Germany, 1973 p. 114; also in press, *Space Res.*, Vol. XIV.
48. BERG, O., AND E. GRÜN, Evidence of Hyperbolic Cosmic Dust Particles. *Space Res.*, Vol. XIII, Akademie Verlag, Berlin, 1973, pp. 1047–1055.
49. ALEXANDER, W. M., C. W. MCCRACKEN, AND J. L. BOHN, Zodiacal Dust: Measurements by Mariner IV. *Science*, Vol. 149, 1965, pp. 1240–1241.
50. NAZAROVA, T. N., Solid Component of Interplanetary Matter From Vehicle Observation. *Space Sci. Reviews*, Vol. 8, 1968. pp. 455–466.
51. ALEXANDER, W. M., C. W. ARTHUR, AND J. L. BOHN, Lunar Explorer 35 and OGO 3: Dust Particle Measurement in Selenocentric and Cislunar Space From 1967 to 1969. *Space Res.*, Vol. XI, Akademie Verlag, Berlin, 1971, pp. 279–285.
52. NAUMANN, R. J., D. W. JEX, AND C. L. JOHNSON, *Calibration of Pegasus and Explorer XXIII Detector Panels.* National Aeronautics and Space Administration, Technical Note TRR–321, 1969.
53. O'NEAL, R. L., *The Explorer XXIII Micrometeoroid Satellite*, NASA Technical Note TN–D 4784, 1968.
54. KONSTANTINOV, B. P., M. M. BREDOV, E. R. MAZETS, V. N. PANOV, R. L. APTEKAR, S. V. GOLENETSKII, Y. A. GURYAN, AND V. N. ILLINSKII, Micrometeors in Circumterrestrial Space Observed by "Kosmos 163," *Cosmic Res.*, Vol. 7, 1969, pp. 817–821.
55. KONSTANTINOV, B. P., M. M. BREDOV, E. R. MAZETS, V. N. PANOV, R. L. APTEKAR, S. V. GOLENETSKII, Y. A. GURYAN, AND V. N. ILLINSKII, Micrometeoroid Investigations on the Satellite "Cosmos 135," *Cosmic Res.*, Vol. 6, 1968, pp. 622–632.
56. GREW, G. W., AND C. A. GÜRTLER, *The Lunar Orbiter Meteoroid Experiment.* National Aeronautics and Space Administration, Technical Note D–6266, 1971.
57. COUR-PALAIS, B. G., The Flux of Meteoroids at the Moon in the Mass Range 10^{-8} to 10^{-12} g from the Apollo Window and Surveyor III TV Camera Results. *Lunar Science*, Vol. V, Lunar Science Institute, Houston, 1974, pp. 138–140.
58. HAWKINS, G. S., Impacts on the Earth and Moon, *Nature*, Vol. 197, No. 4869, 1963.
59. NEUKUM, G., Micrometeoroid Flux, Microcrater Population Development and Erosion Rates on Lunar Rocks, and Exposure Ages of Apollo 16 Rocks Derived From Crater Statistics (abs.). *Lunar Science*, Vol. IV, Lunar Science Institute, Houston, 1973, pp. 558–560.
60. KAISER, T. R., The Determination of the Incident Flux of Radio-Meteors II: Sporadic Meteors. *Monthly Notices Roy. Astron. Soc.*, Vol. 123, 1961, pp. 265–271.
61. LINDBLAD, B. A., Luminosity Functions of Sporadic Meteors and Extrapolation of the Influx Rate to the Micrometeorite Region. *Smithsonian Contr. Astrophys.*, Vol. 11, 1967, pp. 171–180; also in NASA SP–135.
62. LATHAM, G., J. DORMAN, F. DUENNEBIER, M. EWING, D. LAMMLEIN, AND Y. NAKAMURA, Moonquakes, Meteoroids, and the State of the Lunar Interior. *Proc. Fourth Lunar Science Conference, Geochimica et Cosmochimica Acta*, Supplement 4, Vol. 3, 1973, pp. 2515–2527.
63. SHOEMAKER, E. M., Origin of Fragmental Debris on the Lunar Surface and the History of Bombardment of the Moon. *Instituto de Investiga-*

ciones Geologicas de la Diputacion Provincial, Vol. XXV, Universidad de Barcelona, 1971.

64. HARTMANN, W. K., Paleocratering of the Moon, Review of Post-Apollo Data. *Astr. Space Sci.*, Vol. 16, 1972, pp. 183–199.
65. SODERBLOM, L. A., AND L. A. LEBOFSKY. Technique for Rapid Determination of Relative Ages of Lunar Areas From Orbital Photography. *J. Geophys. Res.*, Vol. 77, 1972, pp. 279–296.
66. ANDERS, E., R. GANAPATHY, U. KRÄHENBÜHL, AND J. W. MORGAN, Meteoritic Material on the Moon. *The Moon*, Vol. 8, 1973, pp. 1–24.
67. BARBER, D. J., R. COWSIK, I. D. HUTCHEON, P. B. PRICE, AND P. S. RAJAN, Solar Flares, the Lunar Surface and Gas-Rich Meteorites. *Proc. Second Lunar Science Conference, Geochimica et Cosmochimica Acta*, Supplement 2, Vol. 3, 1971, pp. 2705–2714.
68. RANCITELLI, L. A., Personal communication, 1973.
69. CROZAZ, G., R. DROZD, C. M. HOHENBERG, H. P. HOYT, D. RAGAN, R. M. WALKER, AND D. YUHAS, Solar Flare and Galactic Cosmic Ray Studies of Apollo 14 and 15 Samples. *Proc. Third Lunar Science Conference, Geochimica et Cosmochimica Acta*, Supplement 3, Vol. 3, 1972, pp. 2917–2931.
70. BROWNLEE, D. E., W. BUCHER, AND P. HODGE, Micrometeoroid Flux From Surveyor Glass Surfaces. *Proc. Second Lunar Science Conference*, Vol. 3, 1971, pp. 2781–2789.
71. JAFFE, L. D., Lunar Surface: Changes in 31 Months and Micrometeoroid Flux. *Science*, Vol. 170, 1970, pp. 1092–1094.
72. FLEISCHER, R. L., H. R. HART, AND W. R. GIARD, Surface History of Lunar Soils and Soil Columns. *Geochimica et Cosmochimica Acta*, Vol. 38, 1974, pp. 341–484.
73. BHANDARI, N., J. N. GOSWAMI, S. K. GUPTA, D. LAL, A. S. TAMHANE, AND V. S. VENKATAVARADAN, Collision Controlled Radiation History of the Lunar Regolith. *Proc. Third Lunar Science Conference, Geochimica et Cosmochimica Acta*, Supplement 3, Vol. 3, 1972, pp. 2811–2829.
74. GOSWAMI, J. N., AND D. LAL, Cosmic Ray Irradiation Pattern at the Apollo 17 Site: Implications to Regolith Dynamics. *Lunar Science*, Vol. V, Lunar Science Institute, Houston, 1974, pp. 284–286.
75. STORZER, D., AND J. B. HARTUNG, In preparation, 1974.
76. BROWNLEE, D. E., AND R. S. RAJAN, Micrometeorite Craters Discovered on Chondrule Like Objects From Kapoeta Meteorite. *Science*, Vol. 182, 1974, pp. 1341–1344.
77. RAJAN, R. S., D. E. BROWNLEE, AND F. HÖRZ, The Ancient Micrometeorite Flux, *Lunar Science*, Vol. V, Lunar Science Institute, Houston, 1974, pp. 616–617.
78. RUSS, G. P., D. S. BURNETT, AND G. J. WASSERBURG, Lunar Neutron Stratigraphy. *Earth Planet. Sci. Letters*, Vol. 15, 1972, pp. 172–186.
79. ASHWORTH, D. G., AND J. A. M. MCDONELL, Updated Micrometeorite Influx Rates on the Lunar Surface Deduced From New Measurements of the Solar Wind Sputter Rate and Surface Crater Statistics. COSPAR, Konstanz, Germany, May 23 to June 5, 1973; *Space Res.* Vol. 13, pp. 1071–1083.
80. MARCUS, A. H., A Stochastic Model of the Formation and Survival of Lunar Craters: 2. *Icarus*, Vol. 5, 1966, pp. 165–177.
81. OBERBECK, V. R., AND W. L. QUAIDE, Genetic Implications of Lunar Regolith Thickness Variations. *Icarus*, Vol. 9, 1968, pp. 446–465.
82. OBERBECK, V. R., W. L. QUAIDE, M. MAHAN, AND J. PAULSON, Monte Carlo Calculations of Lunar Regolith Thickness Distribution. *Icarus*, Vol. 19, 1973, pp. 87–107.
83. GAULT, D. E., F. HÖRZ, J. B. HARTUNG, AND D. E. BROWNLEE, Mixing of the Lunar Regolith. *Lunar Science*, Vol. V, Lunar Science Institute, Houston, 1974, pp. 260–262; also in *Proc. Fifth Lunar Science Conference.*
84. MOLINA, E. C., *Poisson's Exponential Binominal Limit.* Van Norstrand, Princeton, 1942.
85. HÖRZ, F., E. SCHNEIDER, AND R. E. HILL, Micrometeoroid Abrasion of Lunar Rocks: A Monte Carlo Simulation. *Proc. Fifth Lunar Science Conference*, Vol. 3, 1974, pp. 2397–2412.
86. GAULT, D. E., W. L., QUAIDE, AND V. R. OBERBECK, Impact Cratering Mechanics and Structures. *Shock Metamorphism of Natural Materials*, B. M. French and N. M. Short, eds., Mono-Book, Baltimore, 1968, pp. 87–99.
87. STÖFFLER, D., M. R. DENCE, M. ABADIAN, AND G. GRAUP, Ejecta Formations and Preimpact Stratigraphy of Lunar and Terrestrial Craters: Possible Implications for the Ancient Lunar Crust. *Lunar Science*, Vol. V, Lunar Science Institute, Houston, 1974, pp. 746–748.
88. SCHNEIDER, W., Petrologische Untersuchungen der Bunten Breccie im Nördlinger Ries. *N. Jb. Miner. Abh.*, Vol. 114, 1974, pp. 136–180.
89. HÖRZ, F., Structural and Minerological Evaluation of an Experimentally Produced Impact Crater in Granite. *Contr. Mineral. and Petrol.*, Vol. 21, 1969, pp. 365–377.
90. KING, E. A., J. C. BUTLER, AND M. F. CARMAN, Chondrules in Apollo 14 Samples and Size Analyses of Apollo 14 and 15 Fines. *Proc. Third Lunar Science Conference, Geochimica*

et Cosmochimica Acta, Supplement 3, Vol. 1, 1972, pp. 673–686.

91. McKay, D. S., R. M. Fruland, and G. Heiken, Grain Size Distribution as an Indicator of the Maturity of Lunar Soils. *Lunar Science*, Vol. V, Lunar Science Institute, Houston, 1974, pp. 480–481.
92. Gault, D. E., and J. A. Wedekind, The Destruction of Tektites by Micrometeoroid Impact. *J. Geophys. Res.*, Vol. 74, 1969, pp. 6780–6794.